SYNTHESIS, CHARACTERIZATION, AND PHOTOCATALYTIC ACTIVITY OF TANTALUM OXIDE THIN FILMS

BY

CODY JENSEN

THESIS

Submitted in partial fulfillment of the requirements
for the degree of Master of Science in Chemical Engineering
in the Graduate College of the
University of Illinois at Urbana-Champaign, 2011

Urbana, Illinois

Advisers:

Professor Mark Shannon
Professor David Cahill

ABSTRACT

An increasing demand for a low cost alternative for water disinfection and the recent push for green energy has caused an explosion of research in photocatalysis. While TiO_2 is considered to be the standard for photocatalysis, there are a number of issues that need to be overcome to push photocatalysis into mainstream applications. In an effort to improve the overall reaction rate, a wider energy gap material, such as Ta_2O_5, that provides a higher cathodic potential and more flexibility in shifting the energy gap provides a possible alternative. Ta_2O_5 thin films were synthesized using a sol-gel method and deposited by dip-coating and spin-coating. The thicknesses of the films ranged from 8 nm to 230 nm and were tested to find an optimum thickness based on the quantum efficiency. The photoactivity of the films was measured using a recirculating methylene blue solution. Above 15 nm, the film thickness did not have an effect on the methylene blue degradation rate. To test the premise of being limited by electron-hole transport, the annealing temperature of the films was varied to increase the crystallinity. The films were annealed under a range of temperatures from 450°C to 1200°C. By x-ray diffraction measurements, the grain size of the films was found to be relatively stable from 638°C to 1075°C. The films annealed at 1200°C showed the presence of a TaO phase and lacked any indication of a Ta_2O_5 phase. No correlation between the annealing temperature and photoactivity of the film was found. The photodegradation rate of methylene blue was determined to be limited by surface interactions of the film. A comparison to a TiO_2 film synthesized from Degussa P25 powder was used to compare to the Ta_2O_5 films. The activity was found to be higher for the TiO_2 films. However, the amount of catalyst and surface area of the TiO_2 were unknown and made conclusive quantitative comparisons challenging.

ACKNOWLEDGMENTS

I would like to thank Mark Shannon for providing me with the opportunity to work on this project and for bestowing his enthusiasm for the increasing importance of water. The time and energy he devoted to sharing his knowledge with me is greatly appreciated. I am especially thankful for him allowing me to join his research group when the timing was not ideal. I would also like to thank David Cahill for taking me on as a co-adviser. He was willing to step in on short notice and provide critical insight into the project that could not have been done without him. Finally, I need to thank Glennys Mensing, who has been there to provide me guidance whenever it was needed.

I also wish to express my gratitude to my loving wife, Jennifer, for her patience and support during my time moving between advisers and projects. For assisting me in characterization and analysis, I would like to thank the staff at Frederick Seitz Materials Research Laboratory, specifically Mauro Sardela, Doug Jeffers, and Julio Soares. I would also like to thank Martin Page for helping out with the titanium dioxide work. Finally, none of this could have been carried out without the generous funding from the Construction Engineering Research Laboratory.

TABLE OF CONTENTS

NOMENCLATURE

A	absorptance
c	speed of light in a vacuum
D_p	penetration depth
e^-	electron
h^+	hole
h	Planck's constant (4.136×10^{-15} eV·s)
I	intensity
I_0	incident intensity
I_x	intensity of light after interacting with medium (where $x = A, R, S,$ or T)
k	extinction coefficient
n	index of refraction
$\hat{n}$	complex index of refraction
PC	photocatalyst
QY	quantum yield
R	reflectance
S	scatter (diffuse reflectance)
T	transmittance
α	attenuation coefficient, incident angle
β	exit angle, broadening at the full width at half maximum (Scherrer eqn)
δ	phase gaine
ε	dielectric function
K	shape factor

μ_0	permeability of free space
θ	scattering angle, Bragg angle (Scherrer eqn)
λ	wavelength
ν	wavenumber
ρ	density
τ	crystallite size
φ	angle of incidence
ψ	angle of refraction
ω	frequency

CHAPTER 1 – PHOTOCATALYSIS FUNDAMENTALS AND CHALLENGES

1.1 Introduction

Over the past one hundred years, the density of the population in urban areas has increased exponentially. In 1910, there were an estimated 227 million people living in or around cities, and today that number is around 3.4 billion [1],[2]. This increase has caused an overwhelming burden on current methods for providing clean water. In some areas in the world, half of the population does not have access to improved water sources [3]. This is in large part due to the current methods for dealing with water treatment. Water purification facilities can cost more than one hundred million dollars to build, maintain and staff [4]. The treatment facilities usually have a multi-step approach to cleaning influent water involving a combination of flocculation, sedimentation, filtration and disinfection. These facilities are not economically feasible for rural areas or smaller population centers. Current large-scale disinfection methods involve chemical treatment with chlorine, hydrogen peroxide, or ozonation, and the cost to produce and use these chemicals is prohibitive in developing regions. Furthermore, using chemicals to disinfect water adds additional issues, as disinfection byproducts can result that persist in the supply lines all the way to the point of use. Some of the disinfection byproducts are as harmful as the chemicals that are removed, especially nitrogenous compounds that can form with chlorine.

An alternative method for disinfection and organic removal involves the mineralization of the compounds to CO_2, H_2O, and minerals. Mineralization can occur by oxidation processes, one of such is photocatalysis or photo-oxidation. Photo-oxidation can take place at room temperature and can decompose a wide variety of organic contaminants. The materials used for

photocatalysis are semiconductors that convert light energy into chemical energy. These materials can be self-cleaning, which reduces on-going maintenance.

Titanium dioxide is the current standard of photocatalysts due to its stability, low cost, minimal health concerns, and relativity high photoactivity [6]. However, titanium dioxide still needs ultraviolet (UV) light ($\lambda < 388$ nm) to be activated. This limits the feasibility of using TiO_2 with solar light, as less of the solar spectrum has sufficient energy to activate the photocatalyst [7]. As a result, a large portion of research is being done on moving the activation energy below 3.1 eV ($\lambda > 400$ nm) to allow visible light activation. Different methods are being deployed to accomplish this, from doping photocatalysts with elements such as nitrogen, sulfur or metals to move the band edge, to co-doping with another photocatalyst, or using an entirely different photocatalyst other than TiO_2. Many potential photocatalysts have issues such as self-corrosion under light, instability in water, or leaching into the solution. This limits the pool of acceptable photocatalysts, or requires special coatings to protect the unstable surfaces.

1.2 Photocatalyst Fundamentals

A photocatalyst is a semiconducting material with an energy gap that is usually between 2.5 and 4.0 eV. Semiconductors with energy gaps below this range do not have the necessary potential to react with materials in water, while semiconductors that have an energy gap above 4 eV requires a high energy photon that is inefficient to create. The photocatalysis process involves multiple steps, some of which having a low probability of occurring. These steps are light absorption, electron-hole excitation, charge transport to the surface and then redox reactions with reactants (Figure 1.1). The final step of the process involves two reactions needing to occur

nearly simultaneously to prevent charge buildup. Any accumulation of charge would cause recombination of carriers to occur, effectively stopping the photocatalytic process.

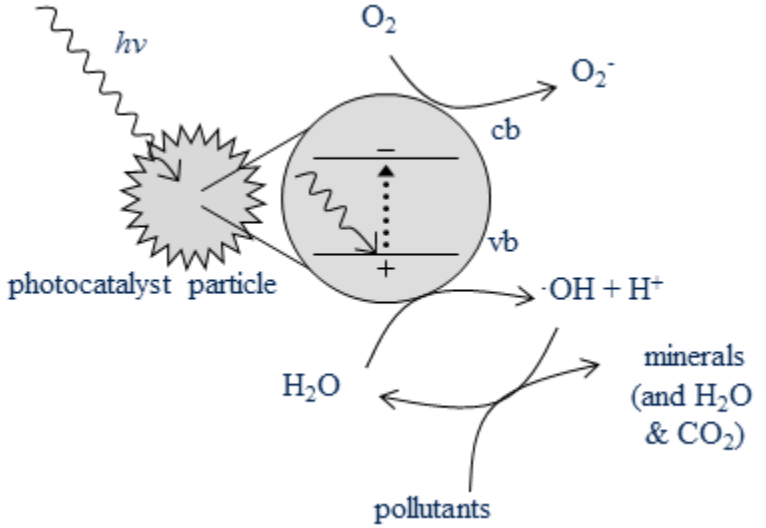

Figure 1.1: Activation of a photocatalyst. For this reaction *hν* must exceed the energy gap of the material, and molecules being reduced (O_2) and oxidized (H_2O) need to be present at the same time [8].

Much of the literature on photocatalyst portrays the photocatalytic reaction as it is shown in Figure 1.1. Unfortunately, there are a few simplifications made for that schematic that can cause confusion or demonstrate a poor understanding of the process. A more accurate, less simplistic representation is shown in Figure 1.2. This schematic shows the reaction taking place on the surface, not in the bulk, as well as the pathway of recombination. Finally, this shows that diffusion is involved in the reaction, and that the electrons and holes do not migrate out into the solution to react as electrons and holes.

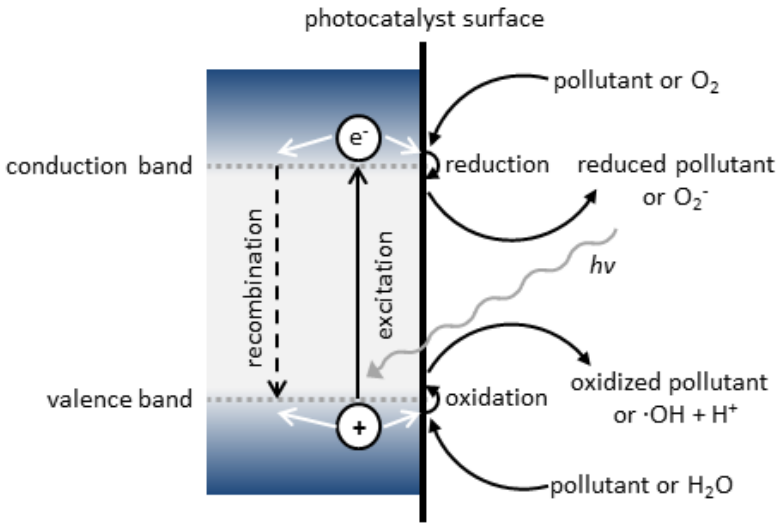

Figure 1.2: Photocatalyst reaction schematic showing diffusion and recombination [9].

The process of photocatalysis can be described by the steps of a chemical reaction pathway through the following generalized reactions [10]:

$$PC + hv \rightarrow PC + e_{CB}^- + h_{VB}^+ \quad 1.1$$

$$e_{CB}^- + h_{VB}^+ \rightarrow heat \quad 1.2$$

$$e_{CB}^- + O_2 \rightarrow O_2^- \quad 1.3$$

$$h_{VB}^+ + H_2O \rightarrow \cdot OH + H^+ \quad 1.4$$

The electrons and holes may react with other species if available, but in an aqueous medium, water is abundant and dissolved oxygen is also present, but to a much lesser extent. Furthermore, some photocatalyst surfaces, such as titanium dioxide, are easily hydroxylated, which will increase the preferential absorption of water on the surface [11].

If the photon has more energy than the energy gap of the semiconductor, it has a probability to excite an electron up from the valence band to the conduction band (eqn. 1.1). This excitation creates and electron-hole pair that can follow three pathways. The first and most common pathway is that the electron-hole pair recombines almost instantaneously, with some

studies estimates ranging from 60 – 90% recombination within nanoseconds of excitation [12],[13]. The recombination can take the form of a photon or thermal energy in the form of multiple phonons being released (eqn. 1.2). The next pathway involves the electron-hole pair migrating in the photocatalyst, but recombining at a defect site or with another electron-hole pair. The final pathway is to migrate to the surface of the photocatalyst where the electron and hole can react with molecules on the surface. If the electron-hole pair reaches the surface of the material, a redox reaction can take place (eqn. 1.3 and 1.4). In an aqueous environment, such as water treatment, the most common oxidant is oxygen and the reductant will be water. The reduced oxygen and oxidized water are only metastable, and will react quickly to return to lose or gain an electron. Most pollutants need to undergo multiple reduction or oxidation reactions before decomposing to H_2O and CO_2 [14],[15]. With each step having a small probability of occurring, many photocatalysts have a quantum efficiency of below 10% and even below 1% [16],[17].

The energy gap of the semiconductor controls what reactions can take place on the surface and what reactions are not thermodynamically possible. Figure 1.3 shows the energy gaps of some semiconductors, as well as some redox couples of interest for water purification. From the figure, if the conduction band is more negative than the reduction reaction, then the reaction can take place. Similarly, the oxidation reaction can occur if the valence band is more positive than the energy required for oxidation. The difference between the band edge and the reaction is directly proportional to the reaction rate.

A few of the redox couples shown in Figure 1.3 have more impact on the degradation of pollutants than others. The formation of a hydroxyl radical (·OH) takes place at 1.9 V, so any photocatalyst with a valence band that is more positive can form hydroxyl radicals. The

formation of hydroxyl radicals is important for removing pollutants. Whereas the direct reaction between the photocatalyst and different pollutants would depend on absorption kinetics, hydroxyl radicals are non-selective [10]. The oxidation of organic pollutants is most commonly attributed to the formation of hydroxyl radicals on the photocatalyst surface.

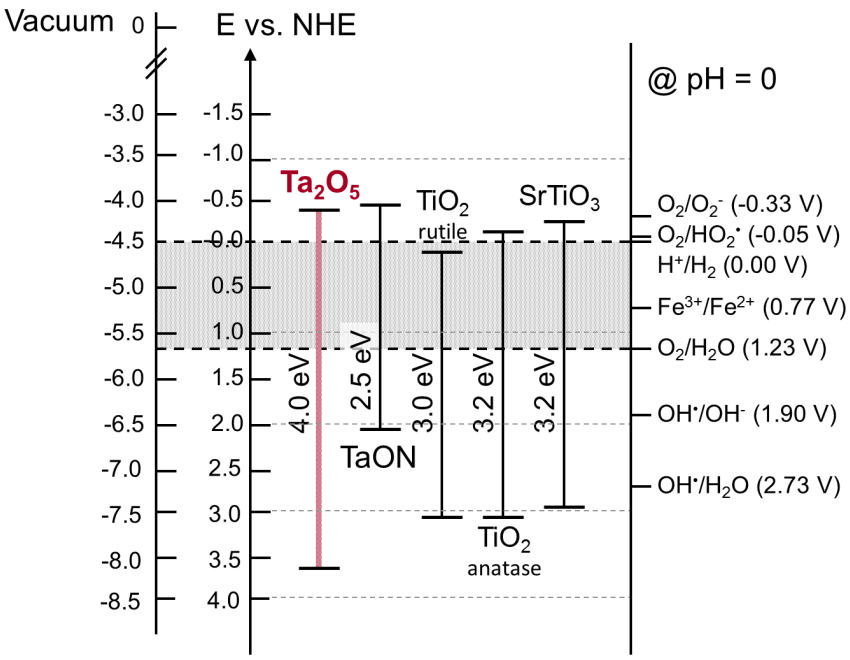

Figure 1.3: Energy gaps of photocatalysts with common redox couples in an aqueous environment. The highlight region contains the lowest amount of energy required for a reaction to take place in water [18].

1.3 Titanium Dioxide or Tantalum Pentoxide

Titanium dioxide shows a high activity due to several important characteristics. The energy gap of TiO_2 is positioned so the valence band has the energy to create a hydroxyl radical from water. However, the conduction band of TiO_2 is only slightly more negative than the reduction of O_2 to $HO_2^{\cdot}$ and should not have the potential to create superoxide (O_2^-) from oxygen. However, previous research has shown that superoxide is present in a measureable amount on TiO_2 surfaces [19]. The photoreaction on TiO_2 is likely limited by the position of the conduction band, since the difference in energy levels is much smaller than on the valence band.

This is evident when reactions are carried out in the absence or low concentrations of oxygen. The reaction rate decreases significantly or stops altogether [20]. This suggests that the reduction of oxygen is the limiting factor of reactions on TiO_2.

Tantalum oxide (Ta_2O_5) is another photocatalyst that has high stability and offers a wider energy gap of ~4.0 eV. The energy required to excite Ta_2O_5 is much higher than TiO_2, but this can be overcome by doping or using a mixed photocatalyst. While it may require more energy, Ta_2O_5 has a conduction band of approximately -0.4 V, which is ~0.3 V more negative than TiO_2. Because of this, not only should Ta_2O_5 have increased kinetics when compared to TiO_2, it has the ability to produce a more aggressive reducing agent, superoxide.

Tantalum oxide has some disadvantages when compared to TiO_2. While it is relatively easy to reduce the energy gap by doping with nitrogen, this will also increase the number of defect sites. Defect sites have been found to either enhance reactivity or act as recombination centers [21],[22]. So doping Ta_2O_5 may reduce the overall activity even if it lowers the activation energy. Additionally, the health effects of Ta_2O_5 have not been investigated as thoroughly as TiO_2 and tantalum oxide is a more expensive compound than titanium dioxide.

Titanium dioxide also requires doping to shift the energy gap into the visible range, so it will suffer from similar issues with defect sites. However, doping the photocatalyst with nitrogen, which lowers the energy gap, does so by moving the valence band [18]. So in the case of n-doped TiO_2, the reduction reaction would still be the limiting reaction. Conversely, Ta_2O_5 has a more negative conduction band, so the overall reaction rate should be higher.

Tantalum oxide as a photocatalyst has been investigated mostly for its potential for hydrogen production by splitting water [23],[24],[25]. This is because Ta_2O_5 and tantalum oxide-derived materials show higher hydrogen production rate than anatase TiO_2 [26]. Tantalum

oxide has been looked at for organic removal as well, but fewer studies exist [27]. I could not find a direct comparison of TiO_2 to Ta_2O_5 involving the decomposition of an organic compound.

1.4 Photocatalysis Research Challenges

Publications on photocatalysis are still showing exponential increases from the mid-90s, with a 20% increase each year since 2000 [28]. However, no standard methods for measuring activity or quantum efficiency currently exist, and because of this, comparisons between two materials is challenging. Some common methods for measuring activity are used in a large number of the literature, such as measuring the degradation rate of dyes by using UV-Vis absorption, or using a gas chromatagraph to measure gaseous degradation. Inconsistencies still exist though, as different dyes are being used and the experimental conditions vary from one research group to another.

The majority of literature involving photocatalysis involves studies of photocatalyst powders. This is advantageous in a laboratory setting, since the activity is much higher due to the higher surface area/mass ratio. However, using a powder presents many challenges in analyzing the results and drawing quantitative conclusions. In a slurry reactor or continuously stirred tank reactor (CSTR), there is the assumption of perfect mixing. In this way, calculations are performed under the assumption that all reactants are in contact with each other. This is typically a valid estimate in liquid phase reactions. However, when this assumption is applied to photocatalysis, it would mean that all photocatalyst particles are receiving an equal amount of light. This is not the case as light is absorbed and reflected as it passes through a medium. In a homogeneous medium, the light intensity should follow $\exp(-\alpha z)$, where α is the absorption coefficient and z is the distance from the source. Since the medium has suspended particles, the

intensity would reduce at a higher rate compared to a homogeneous solution, but would be difficult to accurately measure. Since the amount of light reaching the powders is variable, calculating the efficiency of the photocatalyst becomes difficult. Quantum efficiency measurements are even more challenging, as the total amount of absorbed light is needed. This is usually circumvented by using photon efficiency, which is the number of reacted molecules per photon from the light source. As this estimation does not include the actual light absorption, it will give a quantum yield lower than the true value.

With this in mind, a method for measuring photoactivity that can be reproduced and allows for accurate calculations will be used. A single dye, methylene blue, will be used which is the most common model pollutant used in the literature. Thin films made from photocatalytic materials will be used in lieu of powders. This will make quantum efficiency calculations more accurate, since the films optical characteristics can be measured. Knowing the optical constants, the films can then be made of sufficient thickness to absorb all of the incoming light, simplifying the quantum efficiency calculations. The films will be produced using a sol-gel method. Sol-gel is an inexpensive method that allows control over the structure and stoichiometry, as well as ease of scalability. Additionally, the experimental setup using a film can be scaled up without changes needing to be made to the process. Using a powder will give a higher activity due to the larger specific surface area, but requires immobilization or separation process that can be cost prohibitive. The ability of being able to accurately measure the optical characteristics of the films will be more useful than having a higher activity, allowing for comparisons to be made between films of differing characteristics.

1.5 References

[1] World Urbanization Prospects: The 2005 Revision. United Nations. http://www.un.org/esa/population/publications/WUP2005/2005wup.htm

[2] United Nations, *The World at Six Billion*, Oct 1999.

[3] United Nations, *The Millennium Development Goals Report*, 2010.

[4] water-technolgy.net, *Frank C Amerson Jr Water Treament Facility, United States of America*, 2004. http://www.water-technology.net/projects/bibb/

[5] S.E. Roark, J. Cabrera-Fonseca, M.C. Milazzo, J.H. White, J.D. Wander, *J Environ Eng*, 130 (2004) 329 – 337.

[6] J. Mo, Y. Zhang, Q. Xu, J. Lamson, R. Zhao, *Atmos. Env*, 43 (2009) 2229 – 2246.

[7] C.A. Gueymard, *Sol Energy*, 76 (2004) 423 – 453.

[8] J.M. Herrmann, *Catal Today*, 53 (1999) 115 – 129.

[9] J.M. Herrmann, *App Catal B*, 99 (2010) 461 – 468.

[10] C.S. Turchi and D.F. Ollis, *J Catal*, 122 (1990) 178 – 192.

[11] U. Aschauer, Y. He, H. Cheng, S.C. Li, U. Diebold, A. Selloni, *J Phys Chem*, 114 (2010) 1278 – 1284.

[12] N. Serpone, D. Lawless, R. Khairutdinov, *J Phys Chem*, 99 (1995) 16655 – 16661.

[13] S. Leytner, J.T. Hupp, *Chem Phys Lett*, 330 (2000) 231 – 236.

[14] T. Minabe, D.A. Tryk, P. Sawunyama, Y. Kikuchi, K. Hashimoto, A. Fujishima, *J Photoch Photobio A*, 137 (2000) 53 – 62.

[15] Y. Luo and D.F. Ollis, *J Catal*, 163 (1996) 1 – 11.

[16] R. Asahi, T. Morikawa, T. Ohwaki, K. Aoki, Y. Taga, *Science*, 293 (2001) 269 – 271.

[17] Š. Paušová, J. Krýsa, J. Jirkovský, C. Forano, V. Prevot, G. Mailhot, *Catal Today*, 161 (2011), 140 – 146.

[18] R. Chandrasekharan, *Study of Transport Properties of Ta_2O_5 for high temperature thermal management and photocatalytic water purification systems,* PhD Thesis, University of Illinois – Urbana Champaign, 2008.

[19] J. Schwitzgebel, J.G. Ekerdt, H. Gerischer, A. Heller, *J Phys Chem*, 99 (1995) 5633 – 5638.

[20] S. Malato, P. Fernández-Ibáñez, M.I. Maldonado, J. Blanco, W. Gernjak, *Catal Today*, 147 (2009) 1 – 59.

[21] T. Ihara, M. Miyoshi, Y. Iriyama, O. Matsumoto, S. Sugihara, *App Catal B*, 42 (2003) 403 – 409.

[22] C.D. Valentin, E. Finazzi, G. Pacchioni, A. Selloni, S. Livraghi, M.C. Paganini, E. Giamello, *Chem Phys*, 339 (2007) 44 – 56.

[23] Y. Takahara, J.N. Kondo, T. Takata, D. Lu, K. Domen, *Chem Mater*, 13 (2001) 1194 – 1199.

[24] T. Sreethawong, S. Ngamsinlapasathian, Y. Suzuki, S. Yoshikawa, *J Mol Catal A*, 235 (2005) 1 – 11.

[25] Y. Noda, B. Lee, K. Domen, J.N. Kondo, *Chem Mater*, 20 (2008) 5361 – 5367.

[26] A. Kudo and Y. Miseki, *Chem Soc Rev*, 38 (2009) 253 – 278.

[27] Y. Zhu, F. Yu, Y. Man, Q. Tian, Y. He, N. Wu, *J Solid State Chem*, 178 (2005) 224 – 229.

[28] A. Fujishima, X. Zhang, D.A. Tryk, *Surf Sci Rep*, 63 (2008) 515 – 582.

CHAPTER 2 – THEORY AND EXPERIMENTAL SETUP

2.1 Synthesis

The Ta_2O_5 films were synthesized by a sol-gel process followed by deposition onto silicon <100> or polycrystalline aluminum oxide (Al_2O_3) substrates using either dip coating or spin coating. The sol-gel process used was originally taken from Ndiege *et al.* with slight modifications [1]. The synthesis details are listed in Figure 2.1. I varied the volume of 2-methoxyethanol was varied to change the viscosity to allow a wide range of film thicknesses to be deposited.

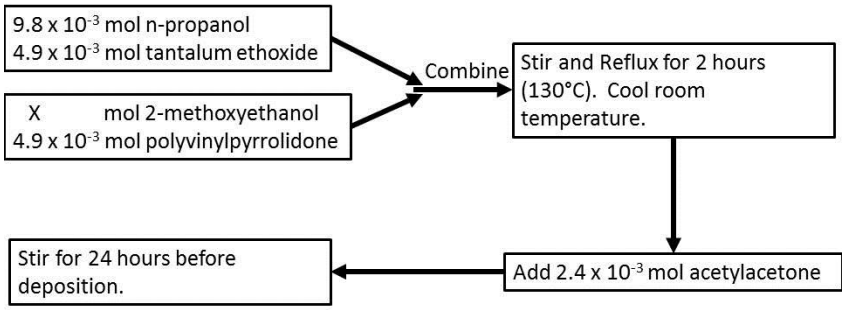

Figure 2.1: Tantalum pentoxide sol-gel synthesis procedure. The value of X for 2-methoxyethanol was varied from 2.6 x 10^{-1} mol to 5.0 x 10^{-1} mol to allow changes in the viscosity to be made.

Tantalum ethoxide was added to n-propanol and stirred for 20 minutes. In a separate container, 2-methoxyethanol and polyvinylpyrrolidone (PVP) were mixed together until all PVP was dissolved. The PVP mixture was added to the tantalum ethoxide mixture slowly by pipetter. A reflux condenser was then connected to the flask, and the mixture was then submerged in an oil. The oil bath was heated to bring the mixture to a boil (~130°C). After two hours of refluxing, the oil bath was turned off and the flask was raised above the bath to cool. When the mixture had cooled to room temperature, acetylacetone was added, and the flask was capped.

The substrates were cleaned in an acetone bath, followed by isopropanol, and then rinsed clean with deionized water. Finally, the substrates were placed in an oxygen plasma for 1 minute

at 100W. For films having a nominal thickness of less than 15 nm, a Chemat Dip Coater-DipMasterTM-50 was used. A single substrate was dipped at a time. The substrate was dipped at a rate of 400 mm/min with a till time of five seconds. The withdrawal rate was varied from 10 mm/min to 20 mm/min to alter the thickness of the films. A BidTec SP-100 spin coater was used to produce films with a nominal thickness greater than 15 nm. The revolution speed was varied from 1500 – 7000 rpm to alter the thickness of the films. Following deposition, the films were air dried for 24 hours before annealing. A Thermal Technology high temperature furnace, Model 1000-4560-FP20, was used for annealing. The films were annealed at 900°C for nine hours in an oxygen-only environment. 1.6°C/min was used for both the heating and cooling rate.

Titanium dioxide films were also produced from a sol-gel. Degussa P25 was used for the TiO_2, which is approximately 80:20 mix of anatase to rutile phase [2]. The 1 g of TiO_2 was added to a solution of 0.5 M titanium isopropoxide and 2.0 M diethanolamine in 100 mL of isopropanol. The solution was stirred for two hours before being dip coated using the above procedure for substrate cleaning and dip coating. The films were then annealed at 400°C for one hour with a heating and cooling rate of 3.3°C/min.

2.2 Characterization

Variable Angle Spectroscopic Ellipsometry (VASE)

A J.A. Woollam VASE was used to find the optical constants and thicknesses of films deposited on Si substrates. The incident angle was varied from 70° to 80°. The optical constants were found at $\lambda = 254$ nm for Ta_2O_5. For film thicknesses, Ψ and Δ values were measured over the range of 500 nm to 1000. The Ψ and Δ values were fit to a model using a Cauchy layer to approximate optical constants of the Ta_2O_5 film.

X-Ray Diffraction (XRD)

The grain size and determination of crystalline phase were obtained by a PANalytical X'pert system with a Cu source. 2-theta spectra were collected on both substrates from 10° to 60°. XRD spectra were then analyzed using MDI's Jade 9.0 software and compared to PDF# 00-025-0922 (*o*-Ta_2O_5) to determine phase information. Grain size, τ, was calculated using the Scherrer equation:

$$\tau = \frac{K\lambda}{\beta cos(\theta)} \quad 2.1$$

where K is the shape factor, λ is the wavelength of the source (1.5405 Å), β is the broadening at the full width at half maximum and θ is the Bragg angle. The β term includes broadening due to both instrumental and strain in the crystalline grain. The instrumental broadening was determined to be ~0.33 and was used in the broadening when calculating the grain sizes.

Rutherford Backscattering Spectroscopy (RBS)

RBS was used to find the areal densities and atomic concentrations in the films. Rutherford backscattering is a nearly nondestructive technique that can show the profile of the film(s) that, unlike other methods such as Auger electron spectroscopy or x-ray photoelectron spectroscopy, does not require sputtering for depth profiling. The data from RBS spectra were fitted to a model that incorporates the number of films present, areal density, atomic concentration, and roughness. A High Voltage Engineering Van de Graaff was used to create a 2.0 MeV He incident particle beam. For each experiment, the parameters of α = 22.5°, β = 52.5°, and θ = 150° were used (see Figure 2.2). A RBS spectrum with a fitted model can be seen in Figure A.3 for a Ta_2O_5 film on a Si substrate and Figure A.4 for an alumina substrate.

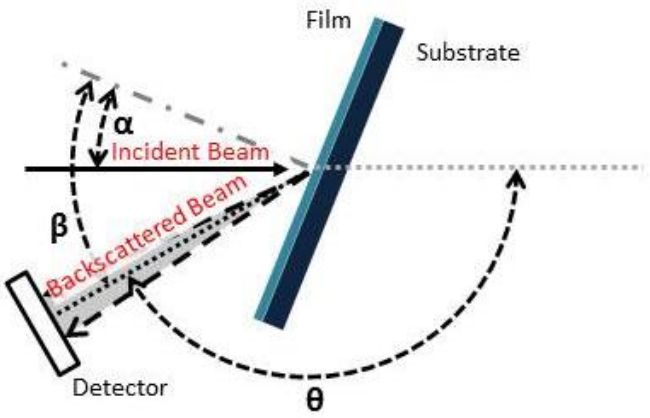

Figure 2.2: RBS experimental setup for thin film characterization with α = 22.5°, β = 52.5°, and θ = 150°.

Photoactivity Experiments

The activity of the Ta_2O_5 films was calculated by measuring the degradation rate of a methylene blue solution. Methylene blue is an organic dye that has been used as a model pollutant [3]. Like most model pollutants, using methylene blue to measure the activity of photocatalyst has some drawbacks. The rate of degradation of methylene is dependent on the pH of the solution, with higher rates being observed in more alkaline solutions [4]. Most model pollutants are fairly large molecules that may require multiple oxidation reactions before being completely mineralized. This can affect the efficiency calculations, since the basis for quantum efficiency is the number of molecules reacted. Another important consideration with methylene blue is that it can undergo photolysis when the incident light is below 350 nm. Although unlikely in the experimental setup used, when methylene blue is in presence of a photocatalyst with a low dissolved oxygen concentration, there is also the possibility of reducing methylene blue to a leucomethylene blue compound [5]. Leucomethylene blue is a colorless compound and would be measured in the same manner as a molecule of methylene blue being oxidized. However, the setup used for measuring the methylene blue concentration using a reservoir was not sealed around the tubing connections to the reservoir. This should allow the dissolved oxygen concentration to remain relatively stable throughout the experiment.

The concentration of methylene blue can be monitored *in situ* during an experiment by measuring the light absorbance at 665 nm. The testing setup used to measure the concentration of methylene blue is shown in Figure 2.3. This setup provides a method to measure real-time concentration changes of methylene blue by using a flow cell. An Ocean Optics LS-1-LL light source, a FIALabs z-flow cell with a 10 mm pathlength, and an Ocean Optics USB4000 spectrometer were used to measure the absorbance of methylene blue. The testing cell underwent several iterations to change the depth of the cell to prevent large bubbles from forming in the testing cell. Any bubble formation would lower the amount of surface area exposed to the solution, as well as cause refraction of the incident light.

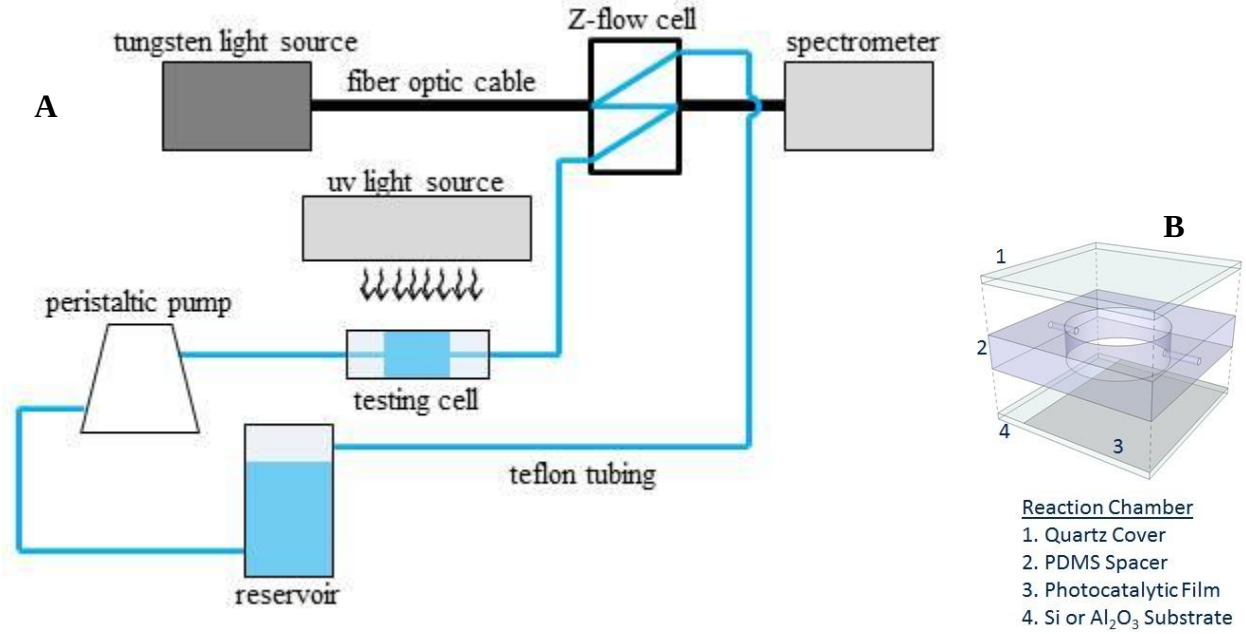

Figure 2.3: Schematic of methylene blue degradation experimental setup (A). UV light source was a handheld low pressure mercury lamp. Close up of testing cell (B).

A 20.0 mL solution was used for each trial with an initial methylene blue concentration of 10 ppm (31.3 μM). A Millipore Direct-Q system was used to produce deionized water with a resistivity of 18.2 MΩ·cm. The solution was recirculated through the system prior to turning on the UV light source to allow the system to equilibrate for 180 minutes. The film was then illuminated and methylene blue degradation was measured for 18 hours. The UV light source

was a 4W, handheld, low pressure, mercury lamp from Spectroline with an intensity of 12.6 mW/cm^2 at λ = 254 nm at the surface of the testing cell (see Figure A.1 for output spectrum). The power was measured using a UV radiometer with a UV-C sensor (230 – 280 nm). The testing cell used had an exposed surface area of 1.77 cm^2 and a total volume of 0.88 mL. Spectrasuite software from Ocean Optics was used to measure the spectra and absorbance of the methylene blue solution.

The degradation rate was calculated by measuring the steady state change in concentration. The absorbance data was converted to concentration using a calibration curve determined from prepared samples of known concentration. The starting solution varied from 9.7 – 10.1 ppm using the calibration curve. The degradation rate was calculated by finding the steady state slope of the concentration over time (ppm was converted to mol for calculations). Linear regression was used between the time of 8 and 18 hours after the light source was turned on. The slope was used as the degradation rate with units of mol methylene blue * hr^{-1}. Uncertainty was determined by calculating the variance between the data and best fit line over the same time frame (refer to Figure A.2).

2.3 Optical Theory

Evaluating the quantum efficiency of a photocatalyst film requires knowledge of the optical characteristics of the film. This section will provide a basic understanding of light absorption and the theory used to calculate the absorptance of a thin film [6].

Optical Constants

The complex index of refraction, $\hat{n}$, is defined as:

$$\hat{n}(\omega) = n(\omega) + ik(\omega) \equiv \sqrt{\epsilon(\omega)} \qquad 2.2$$

where n is the real part of the index of refraction, ω is the frequency, k is the imaginary part, or extinction coefficient, and ε is the dielectric function. For absorbing films, k is responsible for the damping of light waves. The intensity of the light wave in a medium is:

$$I = I_0 e^{-\alpha z} \tag{2.3}$$

where α is defined as:

$$\alpha(\lambda) = \frac{4\pi k(\lambda)}{\lambda} \tag{2.4}$$

The absorption coefficient, α, has units of reciprocal length, so a value called the penetration depth is often used. The penetration depth is the reciprocal of α:

$$D_p = \frac{1}{\alpha} \tag{2.5}$$

A higher penetration depth means the materials has low damping, whereas a material with a low penetration depth has high damping.

Transmission, Reflection, Scattering, and Absorption

When light is impinged onto the surface of a material, the light can follow four pathways (refer to Figure 2.4):

a) reflected specularly (R) at the interface between mediums (air and the thin film)
b) reflected diffusely, or scattered, (S) at the surface or in the second medium (scattered light can leave medium in any direction, including back towards the incoming light or traveling through the sample)
c) transmitted (T) through the sample, maintaining a defined direction
d) absorbed (A) in the medium (not shown in Figure 2.4; occurs only if $k > 0$ for the energy of the incoming light)

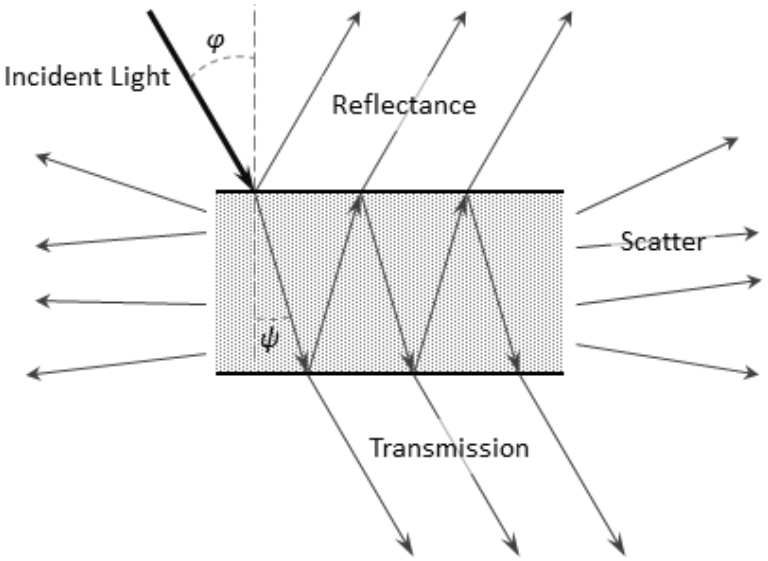

Figure 2.4: Visual definitions of reflectance (specular and diffuse), transmittance. Incident angle is defined as φ.

When light passes from one medium into a second, conservation of energy must be maintained, therefore:

$$T + R + S + A = 1 \qquad 2.6$$

using the following definitions:

$$T = \frac{I_T}{I_0}$$

$$R = \frac{I_R}{I_0}$$

$$S = \frac{I_S}{I_0}$$

$$A = \frac{I_A}{I_0}$$

These quantities are not independent of each other; knowing the value of three provides the fourth quantity. Measuring T and R for bulk samples is a trivial task for spectrophotometers available today, but is usually not possible for thin films. Since thin films typically require a substrate, the transmittance can no longer be measured by placing the sample in the light path.

Even placing the film on a transparent substrate can give cause difficulties if the film shows antireflection properties, yielding a higher transmittance than the reference.

The required theory to calculate T and R for thin films ($A = 0$, $S = 0$) is too lengthy to repeat here, so a condensed form will be presented. Using Snell's law, the angle of refraction can be found from the incident angle and the two indices of refraction:

$$\frac{\sin\varphi}{\sin\psi} = \frac{\hat{n}_2}{\hat{n}_1} \tag{2.7}$$

If the incident angle, indices of refraction for all materials and polarization state of the incident light are known, the Maxwell's boundary conditions for the E and H components of an incoming wave can be applied:

$$E_x^0 + E_x^R = E_x^T \tag{2.8}$$

$$E_y^0 + E_y^R = E_y^T$$

$$H_x^0 + H_x^R = H_x^T \tag{2.9}$$

$$H_y^0 + H_y^R = H_y^T$$

where the superscripts *0*, *R*, and *T* indicate incident, reflected and transmitted waves.

The incoming light wave has a polarization state that changes at an interface. The polarization state has two components, the p component (parallel to the incidence plane), and the s component (normal to the incidence plane). Therefore, for each quantity in 2.8 – 2.9, there is a p and s value:

$$E = E_s + E_p \equiv E_s \boldsymbol{e}_s + E_p \boldsymbol{e}_p$$

After substitution, equation 2.8 can be written as:

$$cos\varphi\left(E_p^0 - E_p^R\right) = E_p^T cos\psi \tag{2.10}$$

$$E_s^0 + E_s^R = E_s^T$$

The quantities in equation 2.9 can be rewritten in terms of the electric field:

$$H_x^0 = -\frac{\hat{n}_1}{\mu_0 c} E_s^0 cos\varphi$$

$$H_y^0 = \frac{\hat{n}_1}{\mu_0 c} E_p^0$$

$$H_x^R = \frac{\hat{n}_1}{\mu_0 c} E_s^R cos\varphi$$

$$H_y^R = \frac{\hat{n}_1}{\mu_0 c} E_p^R$$

$$H_x^T = -\frac{\hat{n}_2}{\mu_0 c} E_s^T cos\psi$$

$$H_y^T = \frac{\hat{n}_2}{\mu_0 c} E_p^T$$

where $\hat{n}_x$ is the complex index of refraction of the medium, μ_0 is the permeability of free space, and c is the speed of light in a vacuum. Substituting these equalities into 2.9:

$$\hat{n}_1 \cos\varphi \, (E_s^0 - E_s^R) = \hat{n}_2 \cos\psi \; E_s^T \qquad 2.11$$

$$\hat{n}_1 \left(E_p^0 + E_p^R\right) = \hat{n}_2 E_p^T$$

Equations 2.10 and 2.11 can then be used to define the unknown values r_s, r_p, t_s, and t_p:

$$r_s = \frac{\hat{n}_1 \cos\varphi - \hat{n}_2 \cos\psi}{\hat{n}_1 \cos\varphi + \hat{n}_2 \cos\psi} \qquad 2.12$$

$$t_s = \frac{2\hat{n}_1 \cos\varphi}{\hat{n}_1 \cos\varphi + \hat{n}_2 \cos\psi} \qquad 2.13$$

$$r_p = \frac{\hat{n}_2 \cos\varphi - \hat{n}_1 \cos\psi}{\hat{n}_2 \cos\varphi + \hat{n}_1 \cos\psi} \qquad 2.14$$

$$t_p = \frac{2\hat{n}_1 \cos\varphi}{\hat{n}_2 \cos\varphi + \hat{n}_1 \cos\psi} \qquad 2.15$$

Equations 2.12 – 2.15 are known as Fresnel's equations. Using Snell's Law (2.7) and the Fresnel equations, the value of R and T can be found knowing the values of $\hat{n}_1$, $\hat{n}_2$, and φ:

$$R = |r|^2 \qquad 2.16$$

$$T = 1 - R = \frac{Re(\hat{n}_2 \cos\psi)}{Re(\hat{n}_1 \cos\varphi)} |t|^2 \qquad 2.17$$

Making the assumption of real refractive indices and a normal incident angle ($\varphi = 0$), 2.16 – 2.17 can be simplified to:

$$R_{12} = \left(\frac{n_1 - n_2}{n_1 + n_2}\right)^2 \quad 2.18$$

$$T_{12} = \frac{4n_1 n_2}{(n_2 + n_1)^2} \quad 2.19$$

Thin films are considered to be a special case, since there are three indices of refraction and the wave in the film gains in phase, δ. When dealing with thin film systems, there are both transmission and reflection interactions occurring at the air-film interface, as well as the film-substrate interface (Figure 2.5).

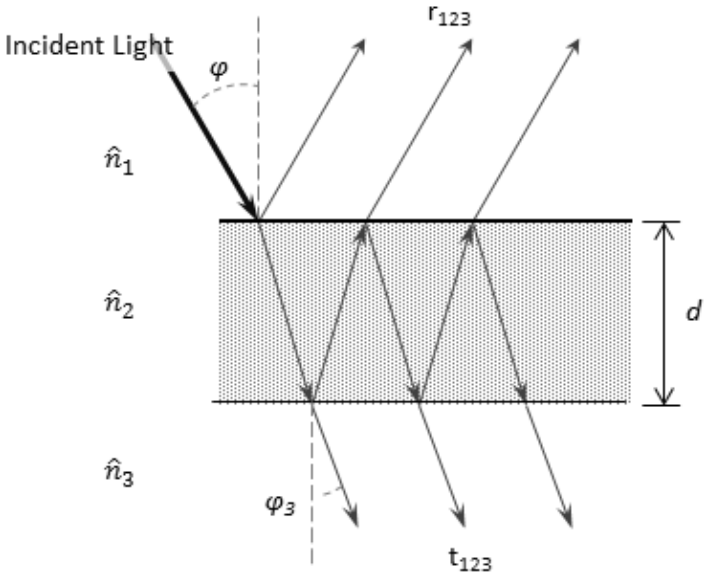

Figure 2.5: Thin film transmittance and reflectance.

Using the subscripts from Figure 2.5, the values of r_{123} and t_{123} can be calculated as:

$$\begin{aligned} r_{123} &= r_{12} + t_{12}e^{i\delta}r_{23}e^{i\delta}t_{21} + t_{12}e^{i\delta}r_{23}e^{i\delta}r_{21}e^{i\delta}r_{23}e^{i\delta}t_{21} + \cdots \\ &= r_{12} + t_{12}r_{23}t_{21}e^{2i\delta}\left(1 + r_{21}r_{23}e^{2i\delta} + \cdots\right) \\ &= r_{12} + \frac{t_{12}r_{23}t_{21}e^{2i\delta}}{1 - r_{21}r_{23}e^{2i\delta}} \end{aligned} \quad 2.20$$

$$t_{123} = t_{12}e^{i\delta}t_{23}\left[1 + r_{21}r_{23}e^{2i\delta} + \left(r_{21}r_{23}e^{2i\delta}\right)^2 + \cdots\right]$$

$$= \frac{t_{12}t_{23}e^{i\delta}}{1-r_{21}r_{23}e^{2i\delta}} \quad 2.21$$

The phase gain, δ, is defined as (see reference for complete derivation):

$$\delta = 2\pi\nu d\sqrt{n_2^2 - sin^2\varphi} \quad 2.22$$

The overall reflectance, *R*, and transmission, *T*, can be found by substituting the values in 2.20 – 2.22 into 2.16 – 2.17:

$$R = |r_{123}|^2$$

$$T = \frac{Re(\hat{n}_3\cos\varphi_3)}{Re(\hat{n}_1\cos\varphi)}|t_{123}|^2$$

Making the assumptions of a homogenous material with a flat surface (S = 0), the absorptance can be found from 2.6:

$$A = 1 - T - R$$

This equation was used to calculate the absorptance curve of a thin film of Ta_2O_5 on Si (Figure 2.6). The assumption of a flat surface was not accurate for the films produced, but shows a maximum absorptance that can be expected. The curve does not approach zero, but instead has an asymptote around 4.5%. This value is limited by the reflectivity of the film.

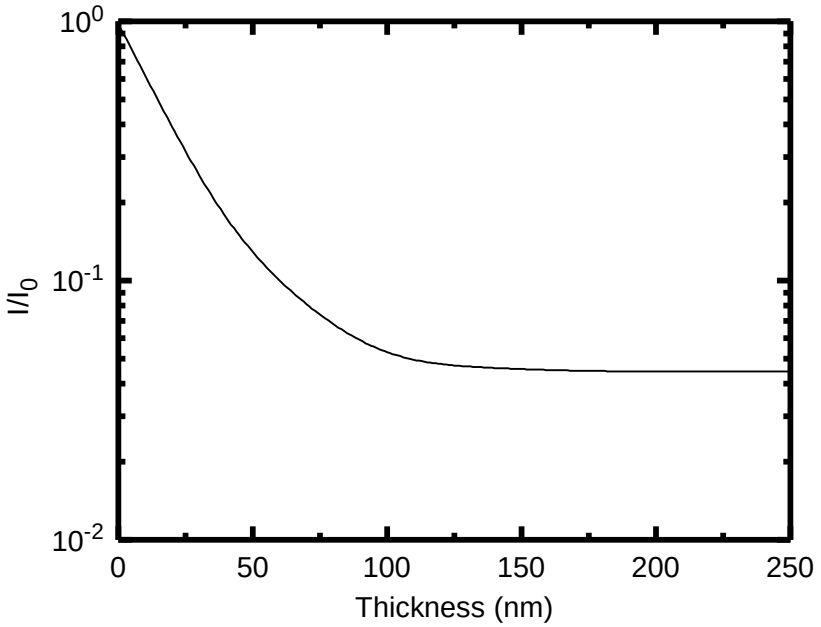

Figure 2.6: Absorptance curve for Ta_2O_5 film on Si at λ = 254 nm. I/I_0 calculated as 1 – *A*, or $I/I_0 = T + R$ using optical constants found from ellipsometry.

2.4 References

[1] N. Ndiege, T. Wilhoite, V. Subramanian, M.A. Shannon, R.I. Masel, *Chem. Mater*., 19 (2007) 3155-3161.

[2] R.I. Bickley, T. Gonzalez-Carreno, J.S. Lees, L. Palmisano, R.J. Tilley, *J Sol State Chem*, 92 (1991) 178 – 190.

[3] G. Sivalingam, K. Nagaveni, M.S. Hegde, G. Madras, *App Cat B*, 45 (2003) 23-38

[4] A. Houas, H. Lachheb, M. Ksibi, E. Elaloui, C. Guillard, J.M. Herrmann, *App Catal B*, 31 (2001) 145 – 157.

[5] T. Zhang, T. Oyama, A. Aoshima, H. Hidaka, J. Zhao, N. Serpone, *J Photochem Photobiol A*, 140 (2001) 163 – 172.

[6] O. Stenzel (2005). The Physics of Thin Film Optical Spectra: An Introduction. Springer-Verlag, Berlin.

CHAPTER 3 - RESULTS AND DISCUSSION

The procedure from Ndiege was previously used to create powders from the sol-gel. With the transition to thin films, some optimizations were required to determine the synthesis conditions that will yield the film with the highest activity based on quantum efficiency. The dependence of the photoactivity on the thickness of the film was measured using the methylene blue degradation rate as the indicator of photoactivity. From the results of thickness optimization, another study was performed to attempt to change the photoactivity by varying the crystallinity of the films.

3.1 Thickness Optimization Results

Ellipsometry Measurements

Using the VASE, the thickness of the synthesized films ranged from 8 to 13 nm for films deposited by dip coating and 17 nm to 230 nm for films deposited by spin coating. Additionally, the optical constants of the Ta_2O_5 films were determined to allow the comparison of the optical depth with the thicknesses produced. The optical constants at λ = 254 nm were n = 2.7 and k = 0.55, which results in D_p = 37 nm. 254 nm was used since it is the same wavelength as the excitation source.

Ellipsometry could only be used for the films on the silicon substrates because of the diffuse surface of the Al_2O_3 substrates. Due to this, comparisons between Si and Al_2O_3 could not be drawn based on optical film thicknesses.

Rutherford Backscattering Spectroscopy (RBS)

RBS provides a method that compares between different thicknesses on the Si and Al_2O_3 substrates. By characterizing the films with RBS, the areal densities can be used to compare the

amount of Ta_2O_5 in the different films. From the RBS data, almost all of the films had a roughness on the same magnitude as the film thicknesses (see Figure 3.1). There was not a discernible difference in film roughness due to the substrate. Both substrates showed a general decrease in roughness with film thickness.

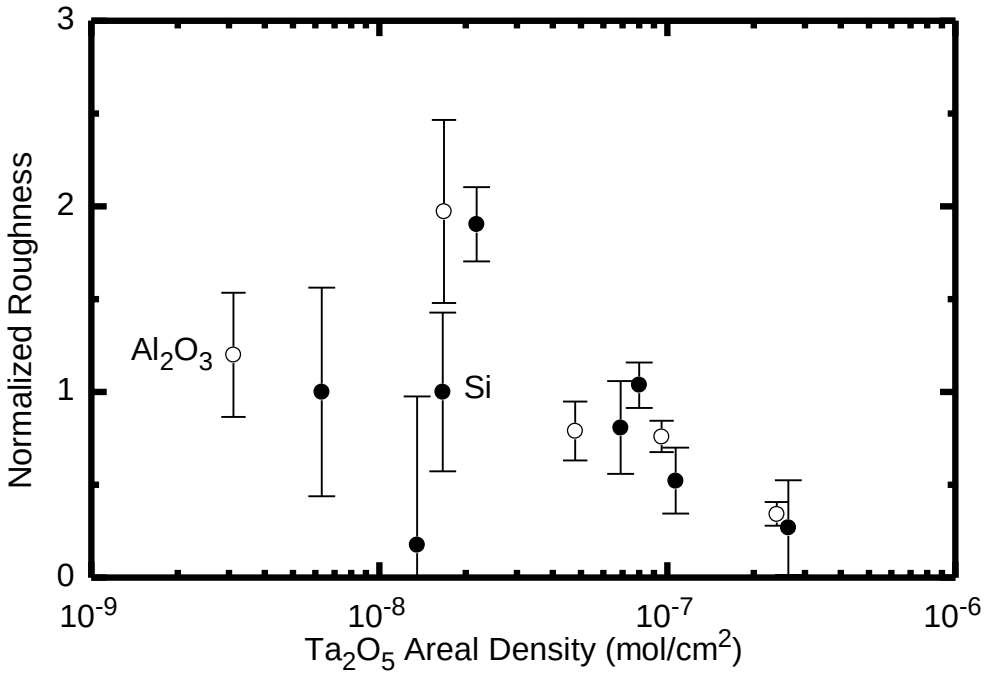

Figure 3.1: Roughness of Ta_2O_5 films by RBS measurements. Normalized roughness calculated as the roughness of the film as a fraction of the thickness of the film.

The areal densities of the films are shown in Figure 3.2 for the thicknesses measured on the silicon substrate. The films that were deposited by dip coating show a higher variance than the films that were made using the spin coater.

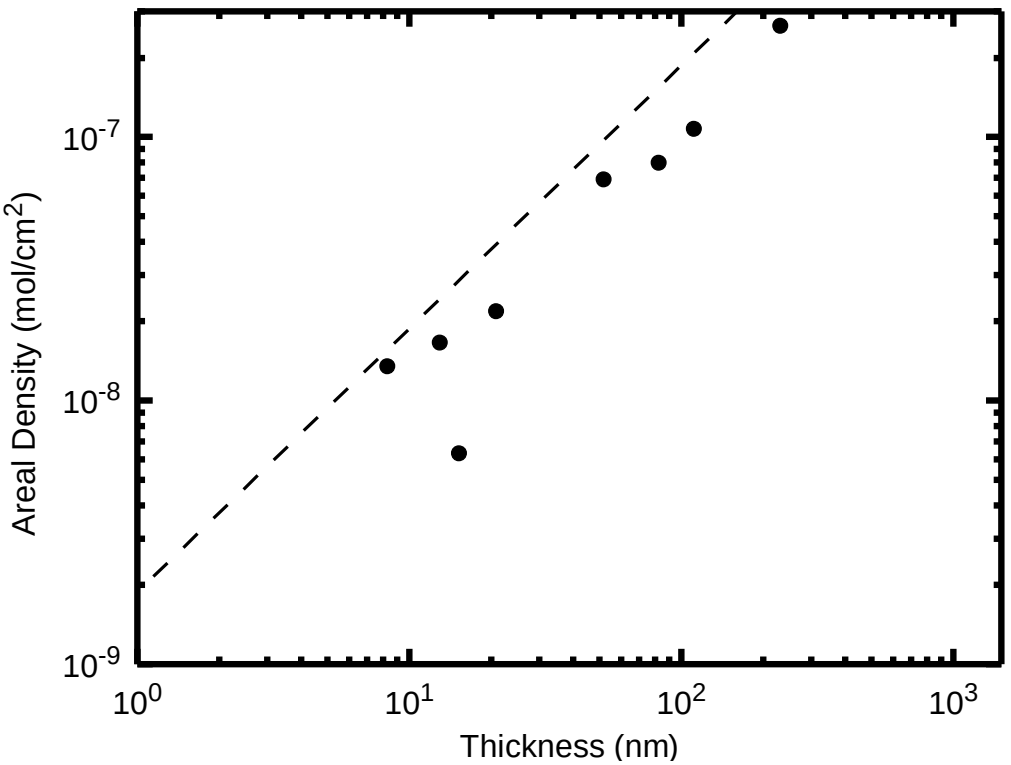

Figure 3.2: Areal density of Ta_2O_5 films as measured by RBS on Si substrate. Optical thickness measured using spectroscopic ellipsometry. Dashed line shows the thickness using the bulk density value for Ta_2O_5 (ρ = 8.2 g/cm^3).

Photoactivity measurements

The effect of the recirculation rate was measured in Figure 3.3. From the data, there was a maximum activity measured at ~7 mL/min. The slight drop off above 7 mL/min is unexpected, as previous studies have shown that the photo-oxidation rate increases with flow rate for photo-reactors [1],[2]. At turbulent conditions, the reaction rate should level off, but increasing turbulence should have no effect on the reaction rate. Another group found no observable change in the reaction rate for flow rates tested [3]. A flow rate of 7 mL/min was chosen for the remainder of the tests. This flow rate resulted in a residence time of approximately 8 s.

The degradation of methylene blue is shown in Figure 3.4 over some of the Ta_2O_5 films on silicon. To verify the degradation seen was not absorption, a negative control was run without the UV-C light present. Additionally, a control run was performed that measured the photolysis

of methylene blue in the presence of UV-C light with no Ta_2O_5 film present. Both controls showed no measureable degradation.

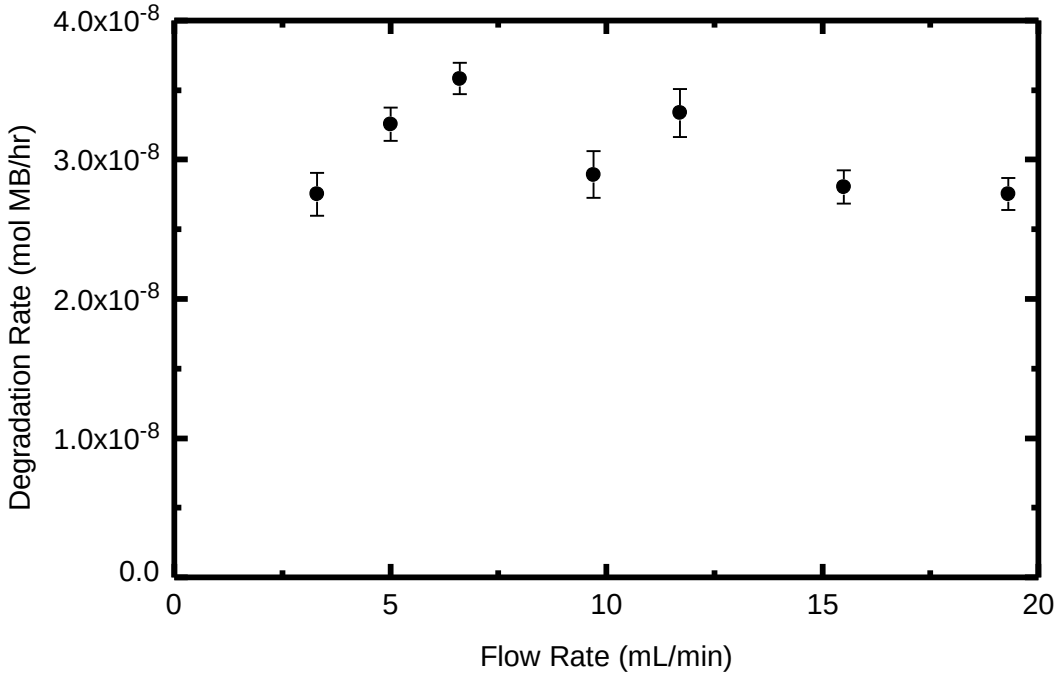

Figure 3.3: Methylene blue degradation over Ta_2O_5 film on silicon substrate. Degradation rate was calculated as the steady state change in concentration over time.

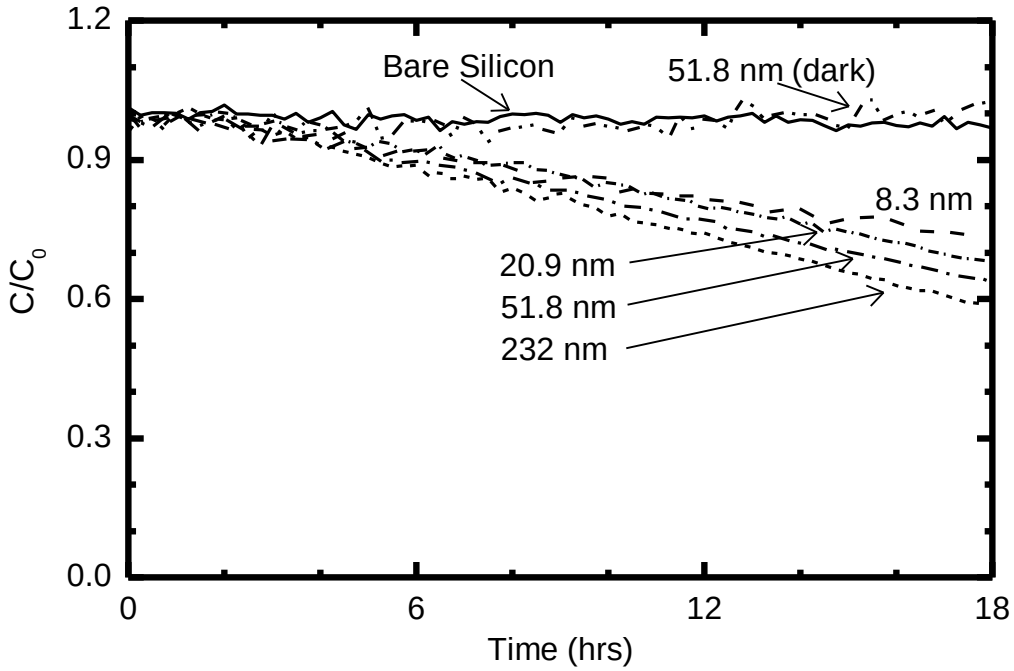

Figure 3.4: Methylene blue degradation rate over Ta_2O_5 films on Si substrates. The vertical dashed line indicates the time at which the light source was turned on, except for the run under dark conditions.

The thickness of the Ta_2O_5 film was varied and the photoactivity was measured by methylene blue degradation (Figure 3.4). The films on the silicon substrate vary from under 10 nm to greater than 200 nm. Only RBS measurements were used to measure the thickness on the Al_2O_3, so only comparisons by areal density will be used between the substrates. The data indicates a plateau in activity above ~$2 \cdot 10^{-8}$ mol Ta_2O_5/cm^2, which corresponds to an optical thickness of 20 nm. Films on the alumina support showed a lower overall activity by ~ 40%.

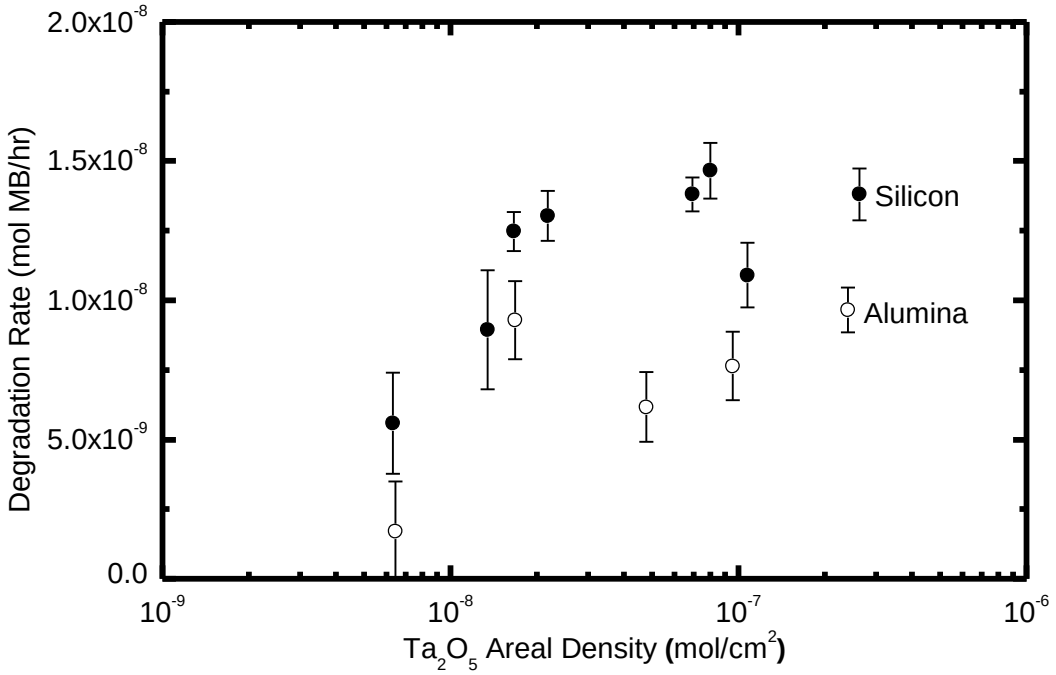

Figure 3.5: Methylene blue degradation rate over Ta_2O_5 films on different substrates. Degradation rates are calculated as the steady state change in concentration with time.

Thickness Optimization Discussion

The results in Figure 3.4 show there is no measured photolysis under the UV-C light. This is in contradiction to a previous finding stating that photolysis will occur below wavelengths of 350 nm [4]. However, there has been other research showing no measureable photolysis under 254 nm, so the exact mechanism is still unclear [5].

Using Figure 2.6, a plateau in activity should not occur until the film reaches ~100 nm in thickness, at which point the film would have absorbed greater than 99% of the incident light

(excluding reflection). However, in Figure 3.5 the activity levels off around 15 nm. The difference in light absorbed between 15 nm and 100 nm is nearly 70% of the incident light. This suggests that the amount of photocatalyst is most likely not limiting the reaction, at least not in films thicker than 15 nm.

To investigate the possible limiting factors, the photocatalytic reaction needs to be broken down in separate steps. For a photocatalyst reaction to take place there needs to be five things (see Figure 1.2): a photon of sufficient energy, the photon being absorbed by the film, the electron-hole pair to reach the surface of the photocatalyst, a reductant to combine with the hole, and an oxidant to combine with the electron.

The light source used to excite the photocatalyst has a flux of 13 mW/cm^2 at the surface of the quartz coverglass. That is equivalent to $7.3 \cdot 10^{16}$ photons/s at the surface. Over the period of the experiment, there are $4.5 \cdot 10^{21}$ photons incident on the quartz. Using n_{quartz} = 1.598 (λ = 254 nm), there would be approximately 6% total reflection at both interfaces, so there would be 4.2E21 photons reaching the solution. If each photon were used to degrade a single methylene blue molecule, $7 \cdot 10^{-3}$ mol of methylene blue would be reduced. The starting amount of methylene blue is only $7 \cdot 10^{-7}$ mol, so it would only require five seconds of excitation for the solution to have enough photons to degrade each molecule of methylene blue. From this calculation, photon flux cannot be the sole limiting factor.

The next step in the reaction is that the photon is absorbed by the film. Using the absorptance curve in Figure 2.6, the effects of absorbing the photon can be eliminated by increasing the thickness of the film. At a thickness of 230 nm, the fraction of light being transmitted through the film is less than $3 \cdot 10^{-5}$. The films synthesized are of sufficient thickness

to absorb greater than 99% of the incident light above 100 nm, so this absorption is not the limiting factor.

Looking at electron-hole transport is more challenging than the previous steps. Measuring transport efficiencies is beyond the scope of this project, so previous research will be applied. The creation of a metastable electron-hole pair is very low in some photocatalysts, with quantum yields below 10% being found [6]. The quantum yield is calculated by using only the photons absorbed in the film:

$$QY = \frac{molecules\ MB\ reacted}{photon\ absorbed} \tag{4.1}$$

Using the data from Figure 3.5, the quantum yield ranges from $3 \cdot 10^{-5}$ to $7 \cdot 10^{-5}$ for the Ta_2O_5 films on silicon (see Figure 3.6). Since the thicknesses were not measured for the films on Al_2O_3, no comparisons can be drawn between the two. There is a general trend of decreasing quantum efficiency with increasing film thickness. The observation of having constant methylene blue degradation regardless of thickness has been reported before. Fretwell and Douglas found a similar result over TiO_2 films of varying thicknesses and attributed it to a surface-mediated reaction, but no further investigation was performed [7].

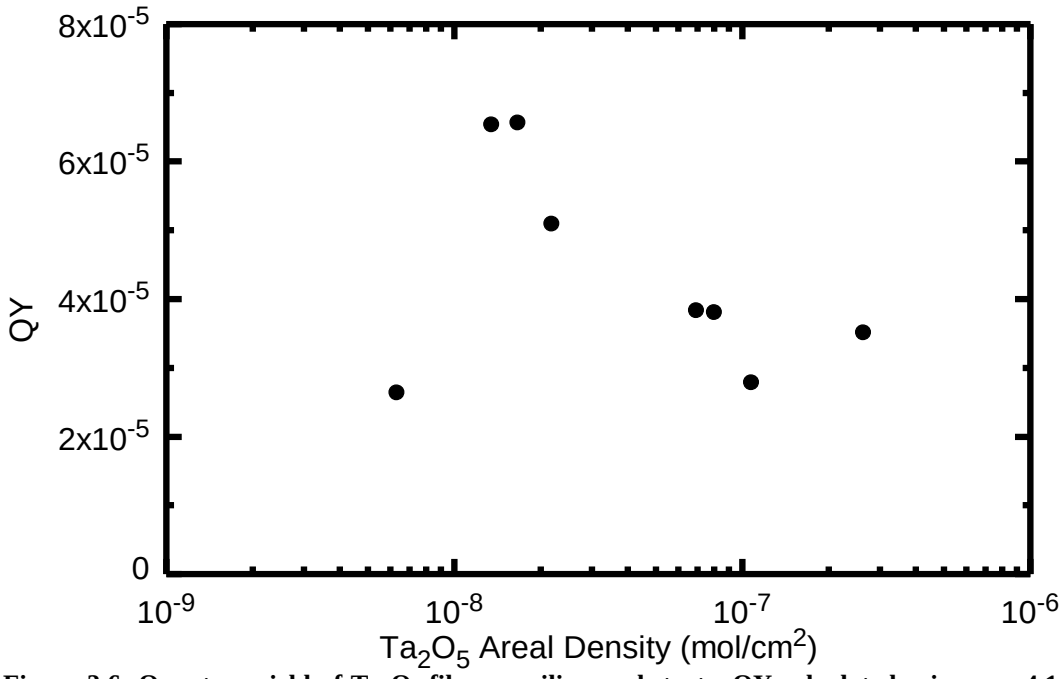

Figure 3.6: Quantum yield of Ta_2O_5 films on silicon substrate. QY calculated using eqn 4.1 and the absorptance curve in Figure 2.6.

The transport of electron-hole pairs is a likely source of the plateau in activity. However, without any data on the transport of electrons or holes in the Ta_2O_5 films, the other steps will be considered first. The redox reactions are limited by the slower reaction to maintain charge balance, so the reactions will be considered together. In an aqueous environment, water is considered to be the reductant and oxygen is the most likely oxidant. Since the solution is more than 99% water, the reduction of oxygen will not be limited by the oxidation of water. Unfortunately, the amount of oxygen could not be measured during the experiments. The system was not sealed though, so it was assumed to hold a relatively constant value over the course of the experiments.

In an attempt to provide some more insight, the degradation experiment was run again with another light source. Table 3.1 shows the degradation rate and intensities from the light sources used. Unfortunately, the difference in the intensities is rather small, so no clear results can be shown. The increase in the degradation rate with a decrease in flux indicates that the

uncertainty in degradation experiments is significant, representing almost a 30% variation after normalizing the intensities.

Table 3.1: Methylene blue degradation over a Ta_2O_5 film on Si. Degradation rate calculated as the steady state change in concentration.

Rated power	Flux* (mW/cm^2)	Degradation Rate (mol MB/hr)
4W	12.7	1.64×10^{-8}
8W	11.1	1.85×10^{-8}

* - flux was measured over 220 – 275 nm

3.2Crystallinity Optimization Results & Discussion

From the experimental data collected, a possible cause of low activity in the films is poor electron-hole separation and transport. Quantitatively measuring the mobility and concentration of electron-hole pairs is outside of the scope of this research. However, other variables can be measured that are qualitatively connected to the carrier mobility. Carrier mobility in semiconductors is limited by interfacial traps [8]. These traps act as potential wells trapping the carriers until they recombine or escape by tunneling [9]. These interfacial traps exist near grain boundaries, dividing a semiconductor into areas of high mobility in the crystalline grains and low mobility at grain boundaries. Using this information, measuring the grain size of the Ta_2O_5 films could provide insight into the transport properties of Ta_2O_5 films.

In an effort to modify the grain size of the films, a study was performed measuring the activity of the films as a function of annealing temperature. Increasing the temperature that Ta_2O_5 is annealed at should produce a polycrystalline films with larger grain sizes, and fewer grain boundaries [10]. The annealing temperature was varied from 450°C to 1200°C for nine hours with a heating and cooling rate of 1.6°C/min. The upper limit of 1200°C was chosen to avoid any issues creating the high temperature phase of tantalum oxide that occurs above 1300° [11].

The methylene blue degradation rate should increase with increasing grain size, but the data in Figure 3.7 does not show a clear correlation between the annealing temperature and degradation rate. The films on the silicon substrate show a maximum activity at 700°C and the alumina substrate shows a maximum at 950°C. The films on the alumina support, however, show a much smaller variance over the temperature range, with the films annealed from 625°C to 1075°C all having degradation rates within $3 \cdot 10^{-9}$ mol MB/hr of each other.

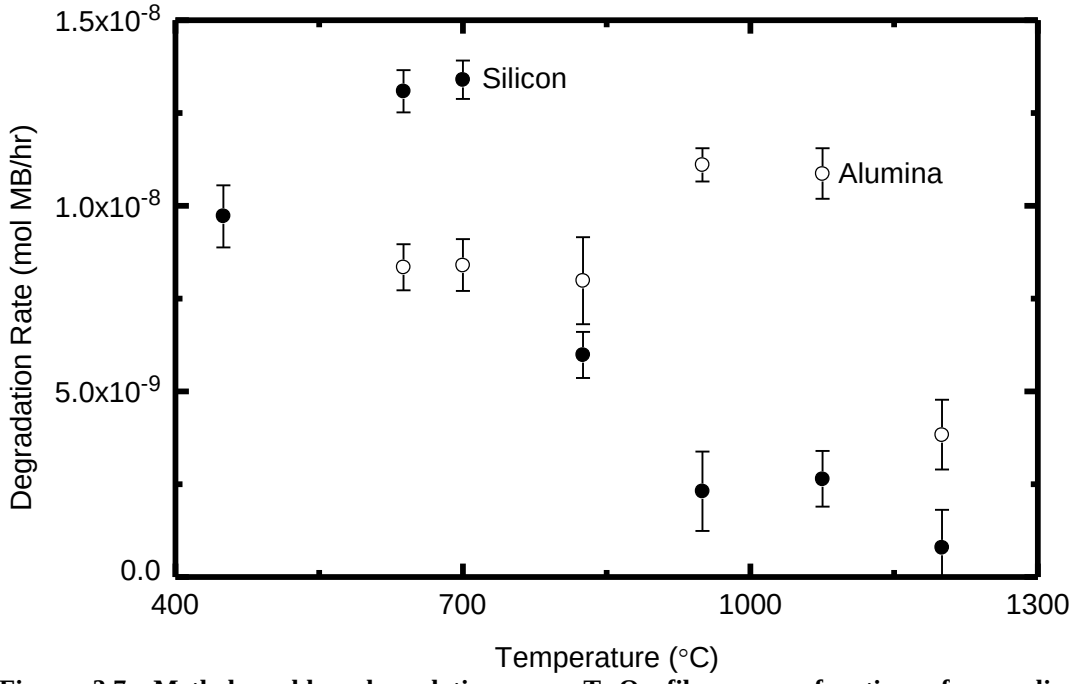

Figure 3.7: Methylene blue degradation over Ta_2O_5 films as a function of annealing temperature.

The films on the silicon substrate have a wide range of activities over the temperature range. The degradation rate at 1200°C is of the same order as the bare substrate. The high temperature shows a decrease in the methylene blue degradtaion, although alumina was only affected at the highest temperature tested.

To determine the cause of the unexpected activity results, XRD analysis was performed on the films. The results show that the grain size was relatively insensitive to annealing temperature (Figure 3.8). The only significant increase in grain size occurs at 1075°C. The data

points from 1200°C were not included, as they did not show the presence of a Ta_2O_5 phase (see Figure 3.10 and Figure 3.11)

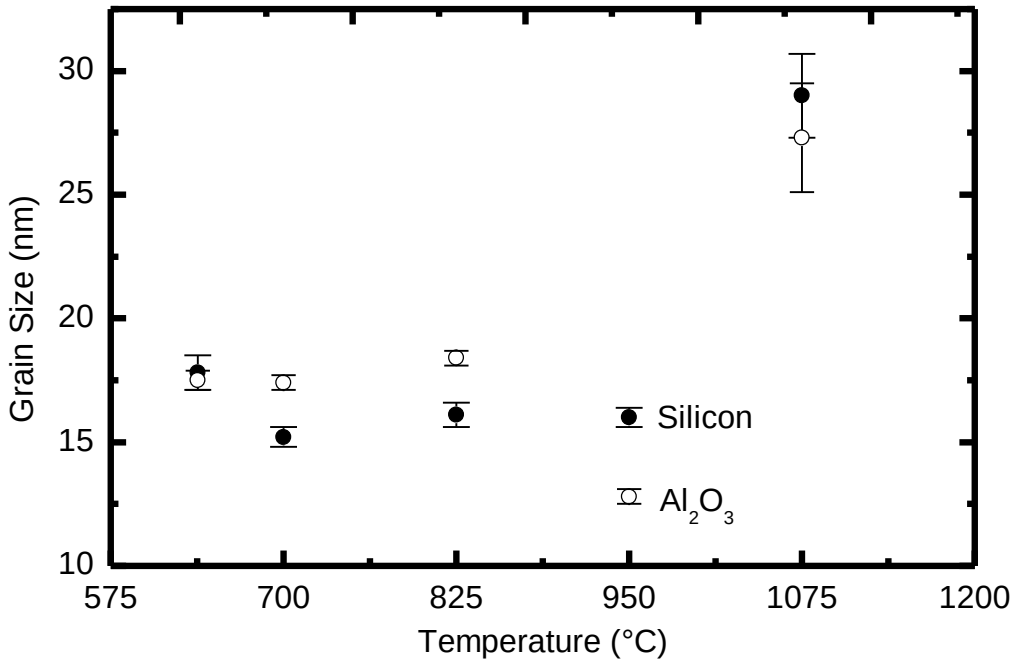

Figure 3.8: Ta_2O_5 grain size as a function of annealing temperature. Grain size calculated using Scherrer equation (eqn 2.1).

The effect of grain size on the degradation temperature is shown in Figure 3.9. As stated previously with the annealing temperature, there is no observable correlation between the grain size and methylene blue degradation rate. Alumina has a range of approximately 15 nm in which the activity did not change appreciably. Silicon, on the other hand, had a wide range of activities over a narrow range of grain sizes. For the silicon substrate, the lowest and highest activity films have a grain size of ~16 nm. The results from both films go against the premise of grain size having an impact on the photoactivity. However, as most of the crystallite sizes were close together and the methylene blue degradation rates were also in a narrow range, there may not be enough data points to state that grain size has no effect on the photoactivity.

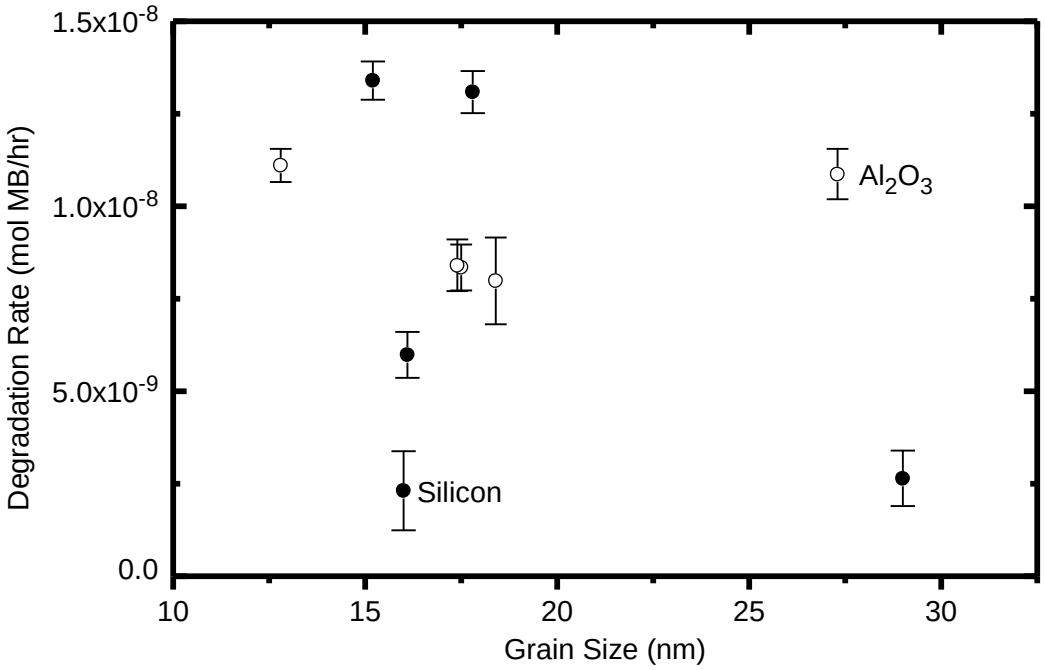

Figure 3.9: Methylene blue degradation as a function of the Ta_2O_5 grain size. Grain sizes taken from Figure 3.8.

Since there is little variation in grain size and there is no apparent correlation between grain size and activity, there must be other factors contributing to the low activity of films annealed at high temperatures on silicon. The XRD spectrum of the films on silicon is shown in Figure 3.10. The Ta_2O_5 film that was annealed at 450°C shows no crystalline phases. This is expected, as the temperature required for crystallization in Ta_2O_5 is above 500°C [12]. From 638°C to 950°C, the only phase present is Ta_2O_5. Above 950°C another phase begins to form. At 1075°C there is a shoulder on the Ta_2O_5 peak at 22.6° and a smaller shoulder on the peak at 28.4°. Then at 1200°C the Ta_2O_5 phase is entirely absent. The peaks present at 1200°C, and to a lesser degree at 1075°C, could be due to a $TaSi_2$ phase or a TaO phase with a stoichiometric ratio of approximately 1:1, judging by the atomic ratios of the phases most similar to the spectrum.

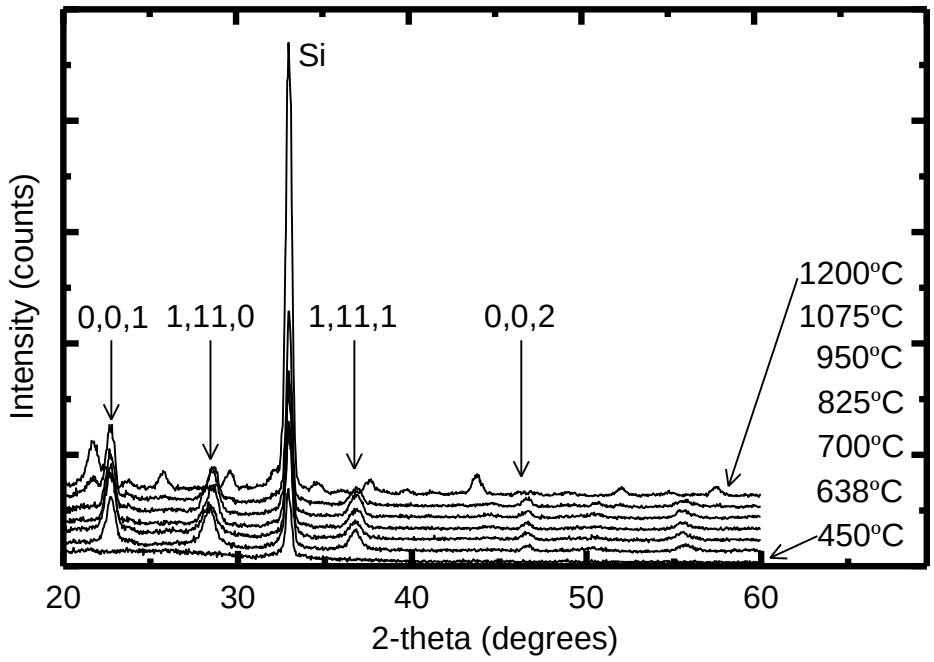

Figure 3.10: XRD spectra of Ta_2O_5 films on silicon substrate. Miller indices are shown for Ta_2O_5 peaks.

The lack of a Ta_2O_5 phase at 1200°C and the presence of additional phases at 1075°C are the most likely cause of the reduced photoactivity. However, this does not explain the activity level of the film at 825°C and 950°C. There is a possibility of lower surface area of the films at high temperatures due to sintering of the material. However, sintering should occur on both substrates, so the fact that alumina lacks a similar reduction in activity may discredit sintering as a possible explanation.

The films on alumina showed less variation with temperature than the silicon substrate. The film at 1200°C had a sharp decrease in activity, similar to the film on silicon. The XRD spectra in Figure 3.11 show the presence of another phase at 1200°C. However, some of the peaks from Ta_2O_5 are still present. Lower temperature films also show additional phases (950°C and 1075°C), but the photoactivity was not affected in the same manner.

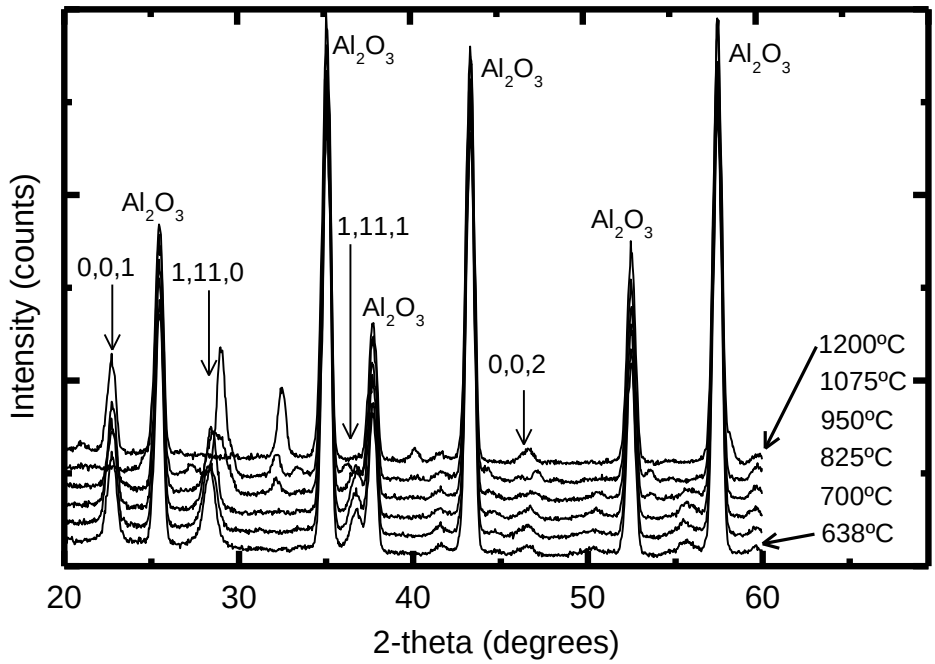

Figure 3.11: XRD Spectra of Ta_2O_5 films on Al_2O_3 substrates. Miller indices of prevalent Ta_2O_5 peaks shown, as well as the peaks from Al_2O_3.

The initial premise of increasing the activity of the film by increasing grain size was not supported by the experimental results collected. However, there was little change in the grain sizes over the annealing temperatures tested. Bertaux *et al.* found a similar result over the same temperature range [13]. Over the temperature range of 700°C to 1200°C, the grain size of the thicker film tested (~140 nm) fell between 25 nm and 28 nm. The results are higher than observed in this study, but that could be attributed to different synthesis methods, as well as annealing procedures.

3.3 Surface-controlled Reactions and TiO_2 Comparison

Almost all of the data collected does not support the initial hypotheses of increasing photoactivity with increasing thickness and increasing activity with increasing annealing temperature. The dependence of activity on film thickness did show a correlation at thicknesses below 20 nm, but this could be due to other factors. For the films less than 85 nm thick, the RBS

spectra showed a significant amount of the substrate material in the top layer. This could be due to either exposed substrate surface or the migration of atoms during annealing. While migration is occurring in the interface, the high roughness values (Figure 3.1) also would suggest that the surface is exposed in some areas.

As the thickness increases for the films with exposed substrate, the surface area would also increase. This would support the previous finding by Fretwell and Douglas that methylene blue photodegradation is surface-mediated. At high thicknesses though, where the substrate is no longer exposed, the surface area would reach a limit dependent on the surface morphology. Since the morphology should remain constant for films created under the same conditions, the surface area should approach a constant value for the Ta_2O_5 films created. The data in Figure 3.5 shows that activity follows the same expected pattern as surface area. Other studies have found similar results with an increase in photoactivity for thin films, but the increase in photoactivity is negligible at higher thicknesses [14],[15].

The idea of methylene blue photodegradation being surface-limited is supported by the data on crystallinity of the films, especially for the films on alumina. The film thicknesses were held constant, so the only variable changed was the annealing temperature. The temperature controlled the grain size and surface area of the films, but the surface area was not measured and was assumed to be relatively constant. This would not be the case due to sintering, but could not be measured. Silicon had a decrease in activity at high temperatures, but the samples at 700°C and below showed consistent activity. For 450°C, there is no crystalline phase present, so the activity should be lower due to the high number of defects [16]. However, if the bulk properties of the sample are not important, the reaction rate would be expected to be similar, supporting a surface-controlled reaction. If the bulk of the semiconductor has no impact on the reaction rate,

then the electron-hole pairs are not able to reach the surface to participate. This would suggest that the recombination is high in the Ta_2O_5 films synthesized. The attempt to decrease defect sites was unsuccessful, though it is still uncertain as to why that was.

While methylene blue did not allow for accurate optimizations to be made concerning film thicknesses, the overall goal was to use tantalum oxide as an alternative to titanium dioxide. The photoactivity data is shown in Figure 3.12 as a function of the areal density of the film. From the data, it is clear that the TiO_2 films have approximately double the activity of any of the Ta_2O_5 films. However, a quantitative comparison cannot be made between the films, since the TiO_2 film was created by suspending a powder into the sol-gel and the surface area is expected to be much higher. The surface area for the unsuspended powder varies from 40 – 50 m^2/g, but is expected to be lower in the film [17]. The average particle size of P25 is 20 nm, which would mitigate any issues found in the Ta_2O_5 films of electron-hole pairs having to travel on the order of 100 nm before reacting at the surface.

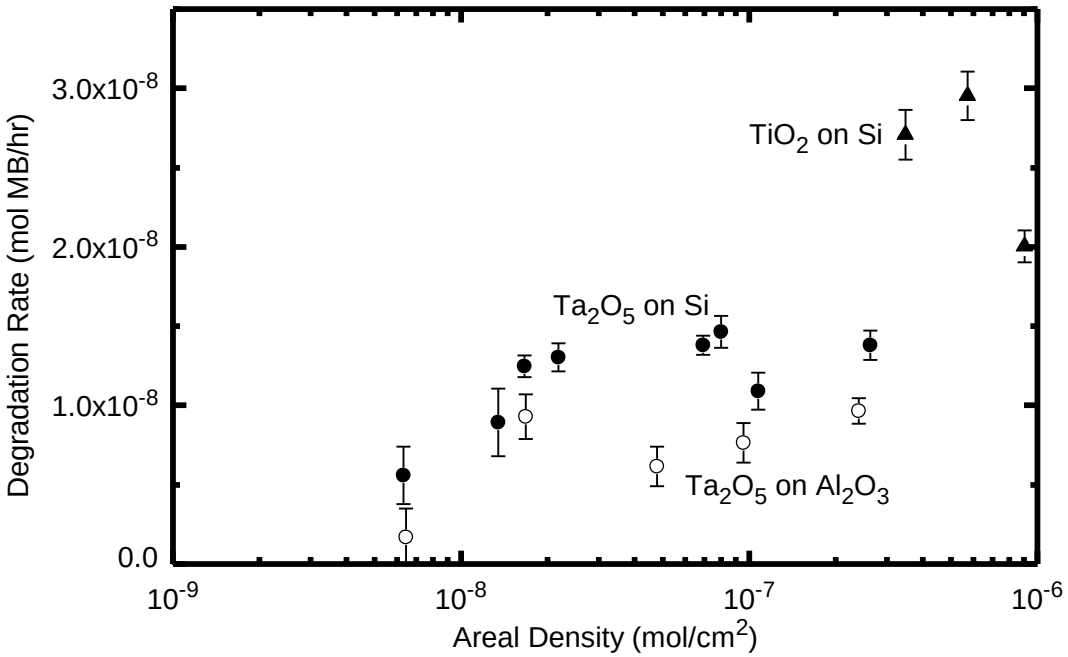

Figure 3.12: Methylene blue degradation over photocatalytic films. A 4W handheld UV-C (λ = 254 nm) light source was used for all films.

3.4 Conclusions

Tantalum oxide thin films have been created using sol-gel synthesis with deposition by spin-coating or dip-coating. The optical properties of the films were characterized using a spectroscopic ellipsometry and a penetration depth of 37 nm was found. The thickness of the films was varied around this thickness from ~8 nm to 230 nm. The films were found to have a high magnitude of roughness by RBS measurements, making comparisons based on thickness difficult. Using the areal density measurements, the correlation between photoactivity and the amount of photocatalyst was made. The photoactivity measurements were performed by monitoring the degradation of methylene blue in solution using a continuous flow setup. From the photoactivity, there was an increase in the methylene blue degradation rate with increasing thickness until ~15 nm, and then the rate leveled off. This was unexpected based on the properties of photocatalysts. Electrons and holes were expected to be able to migrate from the bulk of the material and reach the surface to react. The results suggest that there is little transport occurring in the bulk of the film.

In an attempt to increase the charge transport properties of the Ta_2O_5 films, the films were annealed at increased temperatures to try to increase the grain size. The data showed that the grain size did not change in size dramatically from 700°C to 1200°C. However, there was evidence of another TaO phase forming at higher temperatures on the silicon substrate. The films on the alumina substrate had stable photoactivity over the range tested. No correlation between the change in grain size and photoactivity was found. This supports the premise of methylene blue degradation being limited by the surface excitations of the photocatalyst.

Finally, a comparison between Ta_2O_5 and TiO_2 thin films was made. The results indicated that the TiO_2 films had a photoactivity that was greater than double that of Ta_2O_5.

However, this comparison was only qualitative since the amount of TiO_2 was much higher than any of the Ta_2O_5 samples. Additionally, the TiO_2 films were synthesized by incorporating a powder into a sol-gel. This would give the film a much higher surface area when compared to Ta_2O_5 films. Since methylene blue degradation appears to be dependent on the surface of the photocatalyst, a higher surface area should produce a higher degradation rate. However, no measurements on the surface area were available, and a quantitative comparison between Ta_2O_5 and TiO_2 could not be made.

3.5 References

[1] T. Zhang, T. Oyama, S. Horikoshi, H. Hidaka, J. Zhao, N. Serpone, *Sol Energ Mat Sol C*, 73 (2002) 287 – 303.

[2] R.W. Matthews, *J Chem Soc Farad T 1*, 85 (1989) 1291 – 1302.

[3] C.H. Wu and J.M. Chern, *Ind Eng Chem Res*, 45 (2006) 6450 – 6457.

[4] J. Tschirch, R. Dillert, D. Bahnemann, B. Proft, A. Biedermann, B. Goer, *Res Chem Intermed*, 34 (2008) 381 – 392.

[5] A.M. Ali, E.A.C. Emanuelsson, D.A. Patterson, *App Catal B*, 97 (2010) 168 – 181.

[6] M.D. Hernández-Alonso, F. Fresno, S. Suárez, J.M. Coronado, *Energy Environ. Sci.*, 2 (2009) 1231-1257.

[7] R. Fretwell and P. Douglas, *J Photochem Photobiol A*, 143 (2001) 229 – 240.

[8] G. Horowitz and M.E. Hajlaoui, *Synthetic Metals*, 122 (2001) 185 – 189.

[9] G. Horowitz, M.E. Hajlaoui, R. Haljaoui, *J Appl Phys*, 87 (2000) 4456 – 4463.

[10] M.C. Carotta, M. Ferroni, V. Guidi, G. Martinelli, *Adv Mater*, 11 (1999) 943 – 946.

[11] A.S. Pavlovic, *J Chem Phys*, 40 (1964) 951 – 956.

[12] R. Chandrasekharan, I. Park, R.I. Masel, M.A. Shannon, *J Appl Phys*, 98 (2005), 114908.

[13] S. Bertaux, P. Reynders, J.M. Heintz, *J Euro Cer Soc*, 26 (2006) 923 – 932.

[14] H. Choi, E. Stathatos, D.D. Dionysiou, *Appl Catal B*, 63 (2006) 60 – 67.

[15] P. Zeman and S. Takabayashi, *Thin Solid Films*, 433 (2003) 57 – 62.

[16] J.N. Kondo and K. Domen, *Chem Mater*, 20 (2008) 835 – 847.

[17] R.I. Bickley, T. Gonzalez-Carreno, J.S. Lees, L. Palmisano, R.J. Tilley, *J Sol State Chem*, 92 (1991) 178 – 190.

APPENDIX

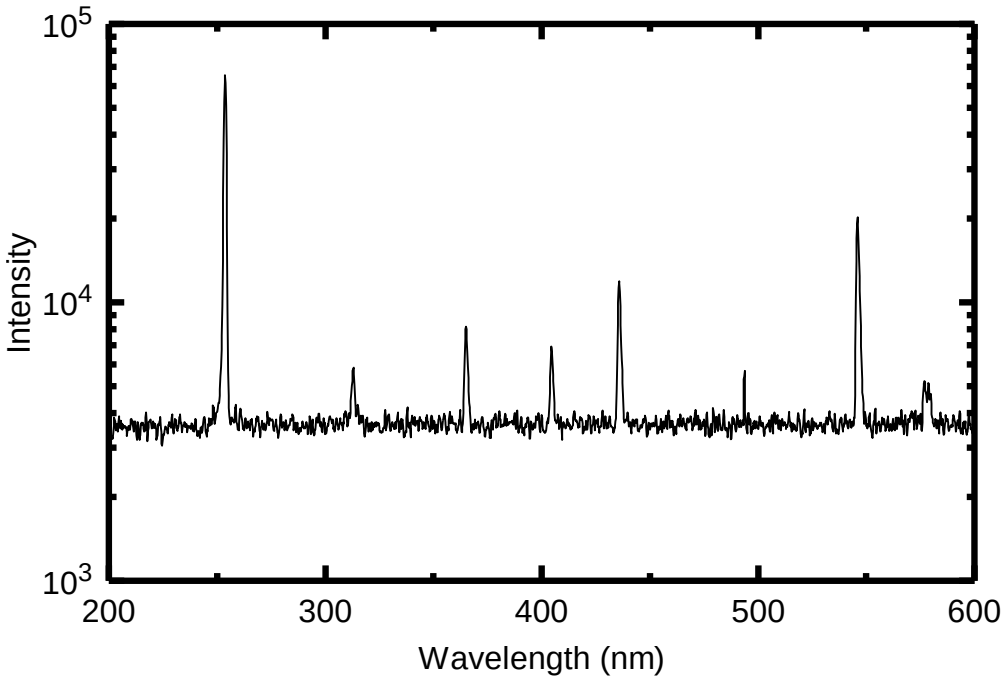

Figure A.1: Spectrum from UV light source used for excitation in photoactivity experiments.

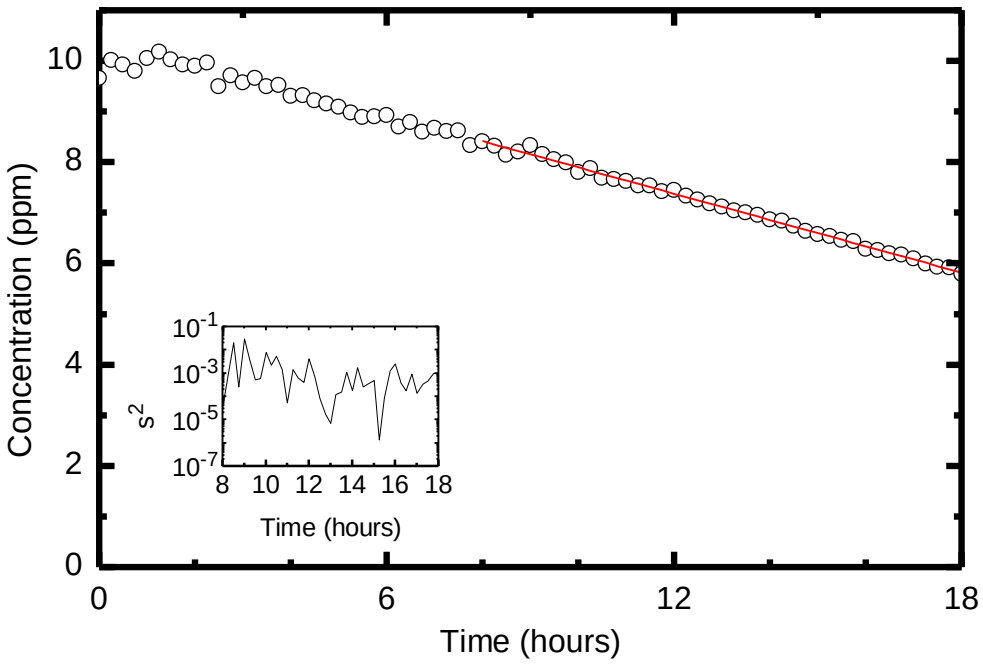

Figure A.2: Degradation of methylene blue over Ta_2O_5 film. Degradation rate calculated from 8 – 18 hours (red line). Inset: variance (s^2) from expected value (degradation rate) and collected data.

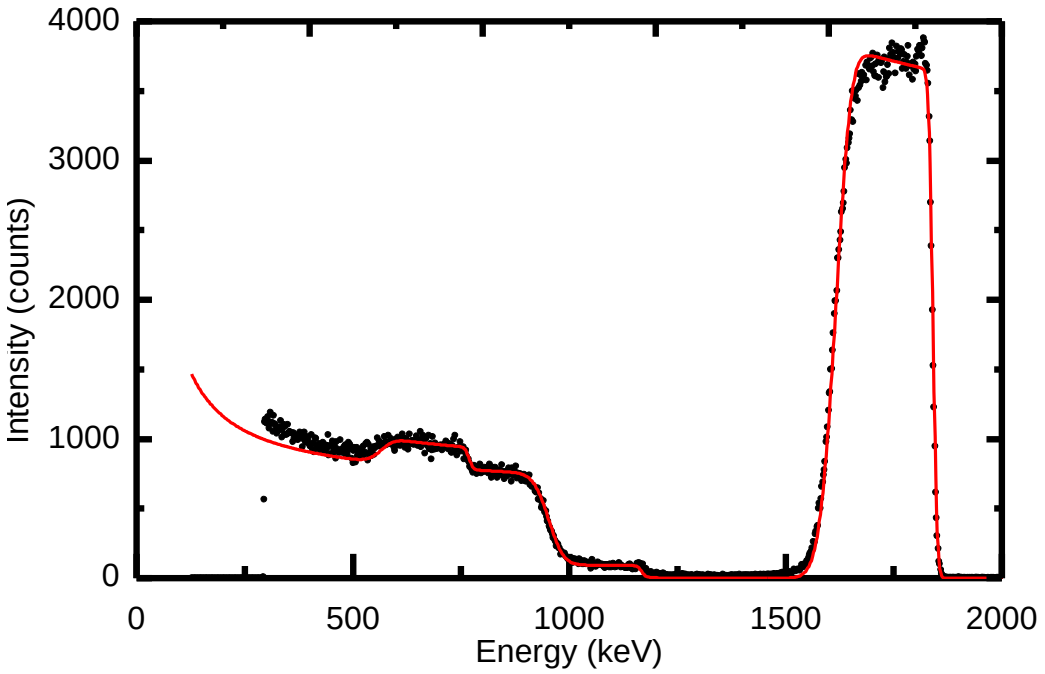

Figure A.3: Rutherford backscattering spectrum of Ta_2O_5 film on Si substrate. RBS experimental setup conditions of α = 22.5°, β = 52.5°, θ = 150° with a 2.0 MeV He source were used. A three layer model was used with a Si substrate, a thin SiO_2 layer and a Ta_2O_5/SiO_2 mixed layer.

Table A.1: Calibration and concentration data used for Figure A.3. Thickness, roughness and atomic values are given in 1E15 atoms/cm^2. The substrate was layer 3, with a Si thickness of 100,000 (1E15 atoms/cm^2).

Calibration Data		Layer 1			Layer 2			Integral (Data)
Offset (keV)	125.0	Ta	19.0%	317.3	Si	33%	20.0	444,034
Energy/Ch (keV/Ch)	1.905	O	68.6%	1,146	O	67%	40.0	Integral (Model)
Particles*sr	1.580e11	Si	12.4%	206.7				443,150
Detector Resolution	18.00							
		Thickness	1,670		60.0			Difference
		Roughness	450					0.20%

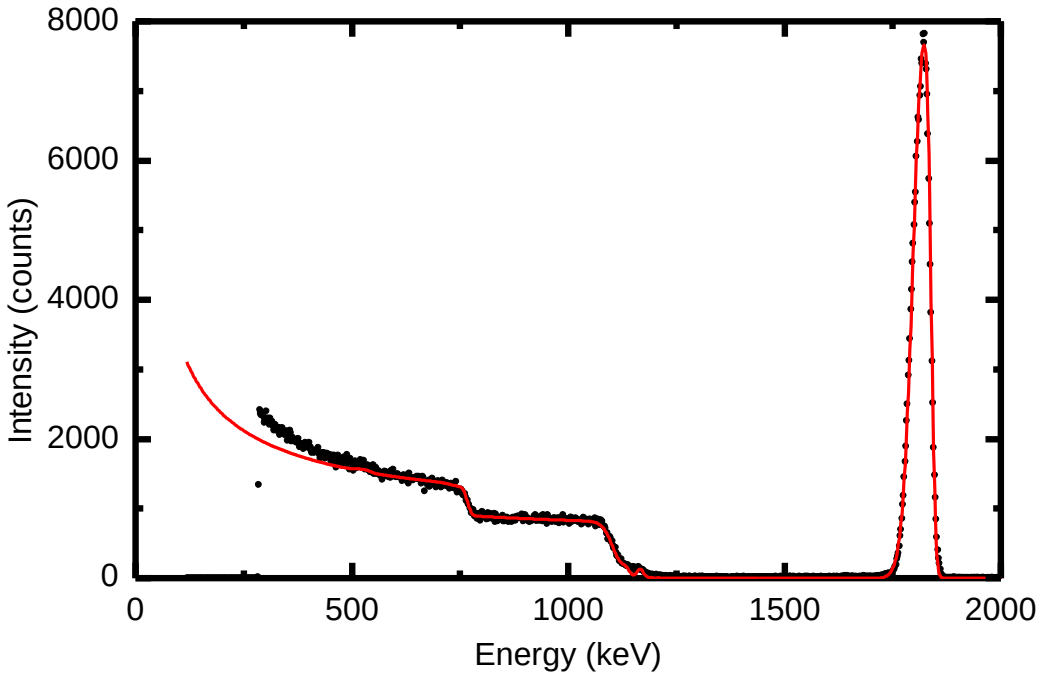

Figure A.4: Rutherford backscattering spectrum of Ta_2O_5 film on Al_2O_3 substrate. RBS experimental setup conditions of α = 22.5°, β = 52.5°, θ = 150° with a 2.0 MeV He source were used. A two layer model was used with an Al_2O_3 substrate and a Ta_2O_5/Al_2O_3 mixed layer.

Table A.2: Calibration and concentration data used for Figure A.4. Thickness, roughness and atomic values are given in 1E15 atoms/cm^2. Silicon in layer 1 is remaining from testing cell (PDMS). The substrate was layer 3 with a ratio of 2:3 Al to O and a thickness of 100,000 (1E15 atoms/cm^2).

Calibration Data		Layer 1			Layer 2			Integral (Data)
Offset (keV)	116.5	Si	100%	12.0	Ta	15.2%	57.8	197,609
Energy/Ch (keV/Ch)	1.891				O	64.0%	243	Integral (Model)
Particles*sr	3.998e11				Al	11.1%	42.2	197,148
Detector Resolution	18.00				C	9.7%	36.9	
		Thickness	12.0		380			Difference
		Roughness			300			0.23%